Journal Pre-proof


# Effects of water discharge on river-dominated delta growth

Zhenhua Xu, Shenghe Wu, Mingcheng Liu, Junshou Zhao, Zhaohui Chen, Ke Zhang, Jiajia Zhang, Zhao Liu

PII: S1995-8226(21)00075-3

DOI: https://doi.org/10.1016/j.petsci.2021.09.027

Reference: PETSCI 66

To appear in: *Petroleum Science*

Received Date: 8 August 2020

Accepted Date: 24 May 2021

Please cite this article as: Xu, Z., Wu, S., Liu, M., Zhao, J., Chen, Z., Zhang, K., Zhang, J., Liu, Z., Effects of water discharge on river-dominated delta growth, *Petroleum Science*, https://doi.org/10.1016/j.petsci.2021.09.027.

Original paper

# Effects of water discharge on river-dominated delta growth

Zhenhua Xu[1, 2], Shenghe Wu[1, 2, *], Mingcheng Liu[1, 2], Junshou Zhao[3], Zhaohui Chen[1, 2], Ke Zhang[1, 2], Jiajia Zhang[1, 2], Zhao Liu[4]

[1] State Key Laboratory of Petroleum Resources and Prospecting, China University of Petroleum-Beijing, Beijing 102249, China

[2] College of Geosciences, China University of Petroleum-Beijing, Changping, Beijing, 102249, China

[3] Bohai Petroleum Research Institute, CNOOC Tianjin Branch, Tianjin 300459, China

[4] Sinopec Geophysical Research Institute, Nanjing, 211103, China

* Corresponding author, E-mail: Reser@cup.edu.cn

Received 08-Aug-2020

Accepted 24-May-2021

Edited by Jie Hao and Teng Zhu

**Abstract:** River-dominated deltas are commonly developed at modern bays and lakes and ancient petroliferous basins. Water discharge is an important variable at pay zone scales in river-dominated delta reservoirs, which affects deltaic sand distributions and evolutions. However, it's unclear how it influences river-dominated delta growth. This paper integrates Delft3D simulations and modern analogs to analyze the effects of water discharge, considering growth time, sediment supply, and coupled effects of sediment properties. High water discharges lead to lobate deltas, and the water discharge of 1,000 $m^3/s$ is a referenced threshold value. Fine-grained, highly-cohesive sediments increase the threshold values of water discharge at which the deltas become lobate from digitate, and vice versa. At the same simulation time, high water discharges favor more rugose shorelines, more distributary channels (especially secondary distributaries), and longer and wider deltas with more land areas. However, at the same sediment supply, high water discharges have few effects on shoreline roughness and the number of distributary channels.

**Keywords:** River-dominated delta; Water discharge; Morphology; Distributary channel; Hydrocarbon exploration

## 1 Introduction

River-dominated deltas are commonly developed at bays and lakes. They can create fertile lands that attract billions of humans to settle down and benefit ecosystems (Woodroffe et al. 2006; Syvitski and Saito 2007; Vörösmarty et al. 2009). Recently, the loss of deltaic wetlands is increasingly severe in the world, which threatens the deltaic habitats, such as Mississippi Delta (Day et al. 2000; Syvitski and Saito 2007; Törnqvist et al. 2008; Syvitski et al. 2009). Human-induced water discharge reduction is a significant reason (Syvitski and Saito 2007; Kim et al. 2009a). It's necessary to understand how the water discharge reduction affects river-dominated delta growth. Besides, river-dominated delta reservoirs are commonly seen in the petroliferous basins, examples as Triassic Yanchang Formation in Ordos Basin (Zou et al. 2010), Paleogene Shahejie Formation (Ji 2008; Zhang et al. 2014; Zeng et al. 2015) and Neogene Minghuazhen Formation (Xu et al. 2019) in Bohai Bay Basin, Cretaceous Yaojia Formation in Songliao Basin (Zhang et al. 2017), Early to Middle Jurassic in Junggar Basin (Fang et al. 2016), and Triassic Xujiahe Formation in Sichuan Basin (Yu et al., 2016). In a similar tectonic setting, water discharge plays an important role in delta evolution. Understanding the effects of the water discharge may help the evolution analysis as well as the inter-well prediction of river-dominated delta reservoirs.

The effects of the fluctuating discharge have been discussed (Edmonds et al. 2010; Piliouras et al. 2017). However, there are still some disputes about the effects of the amount of water discharge on the morphology, number of distributary channels, and deltaic land area of river-dominated deltas. For example, Olariu et al. (2012) suggested that the deltas become elongated during high water discharge periods; Orton and Reading (1993) indicated that low water discharge favors the formation of digitate deltas; Syvitski and Saito (2007) proposed that high discharge can increase the number of channels and deltaic land area. Besides, Edmonds and Slingerland (2010) implied that the deltaic morphology is primarily controlled by sediment properties (grain size and cohesion) and less controlled by water discharge. Fine-grained and highly cohesive sediments lead to digitate deltas with rough shorelines, which are contrasting to lobate deltas with smooth shoreline (Edmonds and Slingerland 2010; Edmonds et al. 2010; Caldwell and Edmonds 2014; Burpee et al. 2015; Tejedor et al. 2016). However, some modern deltas formed by branches of one supplying river present different morphologies, although they have similar sediment properties, such as Wax Lake Delta, Atchafalaya Delta, and Mississippi Delta. These phenomena indicate that the water

discharge may be an important factor that influences the river-dominated delta growth. However, it is still unclear when it comes to the effects of the amounts of water discharge on river-dominated deltas due to the fact that the deltaic growth time and the sediment supply are not considered. The growth time and sediment supply affect delta morphology (such as the number of distributary channels), therefore, it is necessary to compare deltas at the same/similar growth time or sediment supply.

This paper employs simulated and modern deposits to analyze the effect of water discharge on river-dominated deltas considering growth time and sediment supply. The aims of this study are: (1) to quantify differences in morphology, distributary channels, and lands of river-dominated deltas under different amounts of water discharges; (2) to illustrate the significance of water discharge differences coupled with sediments properties. The result of this study can help recognize the significant influences of water discharge on river-dominated delta growth, and help the inter-well prediction of delta reservoirs.

## 2 Methodology

### 2.1 Delft3D simulations

The simulated deltas can be unprecedentedly detailed in terms of growth processes and changes (Hoyal and Sheets 2009; Edmonds and Slingerland 2010), which are proper to reveal the control of water discharge on delta growth. We simulated river-dominated deltas with Delft3D (Version 4.01.01), which is an effective software for delta simulations (Edmonds and Slingerland 2010; Caldwell and Edmonds 2014; Brupee et al. 2015; Baar et al. 2019).

Delft3D adopts a physics-based morphodynamic model based on the numerical fluid-flow and sediment-transport model (Lesser et al. 2004; Marciano et al. 2005). Here, the depth-averaged models are employed, which solve the unsteady shallow water equations horizontally (Tejedor et al. 2016). Neglecting the influences of evaporation, precipitation, Coriolis' force, wind, and waves, the depth-averaged momentum equation in the hydrodynamic model could be expressed as (Lesser et al. 2004; Dissanayake et al. 2009):

$$\frac{\partial \bar{u}}{\partial t}+\bar{u}\frac{\partial \bar{u}}{\partial x}+\bar{v}\frac{\partial \bar{u}}{\partial y}+\mathrm{g}\frac{\partial \zeta}{\partial x}+\frac{\mathrm{g}\bar{u}\left|\sqrt{\bar{u}^2+\bar{v}^2}\right|}{C^2h}-\upsilon\left(\frac{\partial^2 \bar{u}}{\partial x^2}+\frac{\partial^2 \bar{u}}{\partial y^2}\right)=0 \quad (1)$$

$$\frac{\partial \bar{v}}{\partial t}+\bar{u}\frac{\partial \bar{v}}{\partial x}+\bar{v}\frac{\partial \bar{v}}{\partial y}+\mathrm{g}\frac{\partial \zeta}{\partial y}+\frac{\mathrm{g}\bar{v}\left|\sqrt{\bar{u}^2+\bar{v}^2}\right|}{C^2h}-\upsilon\left(\frac{\partial^2\bar{v}}{\partial x^2}+\frac{\partial^2\bar{v}}{\partial y^2}\right)=0 \quad (2)$$

where $\zeta$ is water level, m; $h$ is water depth, m; $\bar{u}$ and $\bar{v}$ are respectively depth-averaged velocity in $x$ and $y$ directions, $m^2/s$; g is gravitational acceleration factor, $m^2/s$; $\upsilon$ is eddy viscosity; $C$ is Chèzy coefficient, $m^{1/2}/s$.

In the Delft3D model, sediments could be divided into suspended load and bedload. Muds (diameter ≤ 64 μm) are considered as cohesive sediments in suspension, whereas sands (diameter > 64 μm) which are considered as noncohesive suspended or bedload sediments. These two types of sediments have different sediment transport models, which can be carried out by the predictor of Van Rijn (1993).

The transport of suspended load sediments is estimated by the 3D depth-averaged advection-diffusion equation, described as:

$$\frac{\partial c_i}{\partial t}+\frac{\partial uc_i}{\partial x}+\frac{\partial vc_i}{\partial y}+\frac{\partial\left(w-\omega_{s,i}\right)c_i}{\partial z}-\frac{\partial}{\partial x}\left(\varepsilon_{s,x,i}\frac{\partial c_i}{\partial x}\right)-\frac{\partial}{\partial y}\left(\varepsilon_{s,y,i}\frac{\partial c_i}{\partial y}\right)-\frac{\partial}{\partial x}\left(\varepsilon_{s,z,i}\frac{\partial c_i}{\partial z}\right)=0 \quad (3)$$

where $c_i$ is the mass concentration of sediment fraction $i$, $kg/m^3$; $u$, $v$ and $w$ are the $x$-, $y$-, and $z$-directed fluid velocities, respectively, m/s; $\varepsilon_{s,x,i}$, $\varepsilon_{s,y,i}$, and $\varepsilon_{s,z,i}$ are the $x$-, $y$-, and $z$-directed eddy diffusivities of sediment fraction $i$, respectively, $m^2/s$; $\omega_{s,i}$ is the settling velocity of sediment fraction $i$, m/s.

The transport of bedload sediments is solved by a formula from Van Rijn (1993), described as:

$$q_{b,i}=0.006\omega_{s,i}D_i\left(\frac{u\left(u-u_{c,i}\right)^{1.4}}{\left(R\mathrm{g}D_{c,i}\right)^{1.2}}\right) \quad (4)$$

$$R=\rho_s/\rho_w-1 \quad (5)$$

Where $q_{b,i}$ is the discharge of bedload sediments per unit width of sediment fraction $i$, $m^2/s$; $R$ is the submerged specific gravity; $\rho_s$ and $\rho_w$ are the specific density of sediment and water, respectively; $u$ is the depth-averaged velocity, m/s; $u_{c,i}$ is the critical depth-averaged velocity for initiation of motion of the sediment fraction $i$, m/s. The direction of bedload transport is determined by local flow conditions and is adjusted for bed-slope effects (Bagnold 1966; Ikeda 1982).

The bed slope effect has an important influence on sediment transport. And parameterizations of

transverse slopes affect the negative feedbacks on over-deepening (Wang et al. 2020). In the predictor of Van Rijn (1993), common parameterizations are by Bagnold (1966) and Ikeda (1982) (Dissanayake et al. 2009). Slope parameterization by Ikeda (1982) is better because it can more efficiently counteract the high incision (Baar et al. 2019).

## 2.2 Linking field observations with Delft3D simulations

Modern delta observations and modelling were linked by using the modern Delta data for simulation parametrization. The simulation domain was a 10 km × 8 km (250 × 200 grid cells) rectangular area (**Fig. 1**). This scale was more than or similar to most of the river-dominated deltas in lakes or bays. The Ganjiang River in Jiangxi Province bifurcated into four branches (West, North, Middle, and South Branch), and formed numerous deltas with different morphologies (digitate or lobate shape) (**Fig. 2**). The supply river scale and basinal topography were based on the data of the Ganjiang River Branches and Poyang Lake, respectively. In the simulations, the supplying river was located in the southern area, with a 280 m width and a 2.5 m depth (**Fig. 1**). The initial river mouth was 2 m in depth. The water basin had a steady downstream slope (~0.046 °) and a constant water level (0 m). Sediment concentrations were all 0.1 kg/m$^3$ (Feng et al. 2017). To illustrate the effect of water discharge, a series of deltas were simulated with steady and different water discharges. Since water discharges of most of supply rivers range from 200–3,000 m$^3$/s (Syvitski and Saito 2007), the water discharge of simulations ranged from 200 to 3,200 m$^3$/s.

**Fig. 1** Map view of the simulation domain. The river mouth was located in the southern area. The supplying river extended into the water basin at the river mouth.

**Fig. 2** Location (a) (After Shankman et al. 2006) and satellite maps (b) of the Ganjiang River Deltas in Jiangxi Province, China, including West / North Branch deltas (c), Middle Branch deltas (d), South Branch deltas (e), and newly formed distal channels within Middle Branch delta (f).

Meanwhile, considering coupled influences of sediment properties, five kinds of sediment mixtures were set by changing sediment cohesion and mud proportions. The sediment cohesion was quantified by critical shear stress ($\tau$) for the erosion of cohesive sediments. The mud

proportion was set by adjusting proportions of sediment fractions which have diameters of 300, 150, 80, 32, 13, 7.5 μm, respectively (the first three are non-cohesive sands and the others are cohesive muds) (Burpee et al. 2015). The proportions of sediment fractions approximately followed the normal distribution. The simulation design was shown in Table 1. The very-coarse-grained type was based on the Wax Lake Delta (Van Heerden 1983) and the fine-grained type was based on the Ganjiang Delta (field work data).

**Table 1** The simulation design.

| Simulations | Mud proportion | Sediment cohesion ($N/m^2$) | Water discharge ($m^3/s$) | Sediment mixture type |
|---|---|---|---|---|
| Sf1–Sf9 | 4 | 2 | 200–3,200 | Fine-grained |
| Sm1–Sm9 | 2.33 | 1.5 | 200–3,200 | Medium-grained |
| Smc | 1.5 | 0.5 | 1,200 | Medium-coarse-grained |
| Sc1–Sc9 | 0.67 | 0.5 | 200–3,200 | Coarse-grained |
| Svc1 | 0.5 | 0.5 | 1,200 | Very-coarse-grained |

To accelerate the simulating speed, the morphological factor was set to be 175, which was an increased rate of morphological change (Burpee et al. 2015). The time step was 0.2 min. Some other parameter settings are shown in **Table 2**. Simulations mostly ran for 360–2,000 h, until the distributary channels, carrying the most of sediments, extended out of the model domain. The 360–2000 simulated hours scaled to 264–1,469 years, in reality, assuming that rivers experience bankfull (i.e., geomorphically effective) conditions which lasted for ~10 days per year (Caldwell and Edmonds 2014).

**Table 2** Simulation parameters for deltas in this study

| Model parameters | Value | Units |
|---|---|---|
| Domain (length × width) | 10 × 8 | km × km |
| Cell size | 40 × 40 | m × m |
| Dimension of supplying river (width × depth) | 280 × 2.5 | m × m |
| Initial water depth of river mouth | 2 | m |
| Slope of basin floor | 0.046 | ° |
| Water level | 0 | m |

| | | |
|---|---|---|
| Initial sediment layer thickness at bed | 10 | m |
| Subsurface stratigraphy bed layer thickness | 0.1 | m |
| Time step | 0.2 | min |
| Morphological scale factor | 175 | - |
| Chezy value for hydrodynamic roughness | 45 | $m^{0.5}/s$ |
| Background horizontal eddy viscosity and diffusivity | 0.001 | $m^2/s$ |
| Factor for erosion of adjacent dry cells | 0.25 | - |
| Total sedimentary concentration within river | 0.1 | $kg/m^3$ |
| Cohesive sediment critical shear stress for deposition | 1,000 | $N/m^2$ |

**Fig. 3** illustrates map views of the simulated deltas with medium-grained sediment mixtures (Sm1–Sm9). The distributary channels and lands could be recognized according to over-time data of water depth and depth-averaged velocity (Shaw et al. 2008; Wolinsky et al. 2010; Tejedor et al. 2015). We defined deltaic land cells as having water depths less than 0.5 m and identified the active channel skeletons as having water depths greater than 1 m and depth-averaged velocities greater than 1.3 m/s. The combined active and abandoned channel skeletons were acquired by overlapping the time-varied active channel skeleton (**Fig. 4**).

**Fig. 3** Map views of water depth of simulations Sm1–Sm9. The water discharges and simulated hours are shown in the upper-right corner.

**Fig. 4** Map views of distributary channels (including active and abandoned channels) in simulations Sm1–Sm9. Red areas are distributary channels and white curves indicate primary distributaries. High discharges resulted in more distributaries (especially secondary distributaries) and more complicated distributary channel networks.

## 2.3 Modern deposit analysis

Modern deposits provide direct evidence and could also be used to exam simulation results. We randomly chose 18 worldwide modern river-dominated deltas to quantify the effects of water discharge on the number of distributary channels and morphology, compared with the effects of mud-proportion (**Table 3**). The dataset was based on references and satellite images.

**Table 3** Datasets of typical modern river-dominated deltas (After Morton and Donaldson 1978; Wang

and Liang 2000; Syvitski and Saito 2007; Edmonds and Slingerland 2010; Yuan et al. 2011; Propastin 2012; Milliman and Farnsworth 2013; Chalov et al. 2017; Chen et al. 2018). The Yellow River Delta and Mississippi Delta include recent and modern deposits.

| Modern river-dominated deltas | Average water discharge($m^3/s$) | Mud proportion | Number of distributary channels | Morphology |
|---|---|---|---|---|
| Selenga River Delta | 1,500 | 3.3 | 30 | Lobate |
| Lena delta | 16,240 | 22.5 | 115 | Lobate |
| Volga Delta | 8,200 | 15.8 | 100 | Lobate |
| Yellow River Delta | 1,480 | 2.8 | 16 | Lobate |
| Mississippi Delta | 15,452 | 11.5 | 71 | Lobate |
| Luanhe Delta | 148 | >0.5 | 10 | Lobate |
| Indigirka River Delta | 1,734 | 5.4 | 28 | Lobate |
| Mackenzie River Delta | 9,750 | 26.3 | 23 | Lobate |
| Nile River Delta | 3,484 | 50 | 15 | Lobate |
| Yukon River Delta | 6,620 | 9.5 | 43 | Lobate |
| Ganjiang Delta (Middle Branch) | 920 | 3.5 | 37 | Lobate |
| Ganjiang Delta (South Branch) | 700 | 3.5 | 21 | Digitate |
| Ganjiang Delta (West / North Branch) | ~250 | 4 | ~ 6 | Digitate |
| Longquanhe Delta | ~50 | 4.9 | 2 | Digitate |
| Karatal River Delta | 91 | - | 2 | Digitate |
| Ili River Delta | 476 | - | 9 | Digitate |
| Ouchi river delta | 300 | - | 1 | Digitate |
| Guadalupe Delta | 93 | 5 | 8 | Digitate |

The adjacent river-dominated deltas formed by different branches of a supplying river are more convincing to verify the effect of water discharges due to similar sediment properties, topography, climate, and basin energy. We chose two examples: one example is the Ganjiang River in China that bifurcated into four branches (West, North, Middle, and South Branch) and extended into the

west side of the Poyang Lake (**Fig. 2**); the other example is the Mississippi River that bifurcated into three branches (Lower Mississippi River, Low Atchafalaya River Outlet, and Wax Lake Outlet) and extended into the Gulf of Mexico (**Fig. 5**).

**Fig. 5** Maps of three modern river-dominated deltas in the Gulf of Mexico. (a) Satellite map of the Gulf of Mexico. (b) Satellite map of the Atchafalaya Delta and Wax Lake Delta. (c) History changes of the Atchafalaya Delta (Modified from Van Heerden 1983). (d) Satellite map of the Mississippi Delta. (e) Satellite map of the Head of Passes of the Mississippi Delta.

## 3 Description and measurement of metrics

We defined several metrics to quantify deltaic morphology, distributary channels, and land areas. Besides, we considered time-varied and supply-varied metrics. To simplify the values of the sediment supply, we defined the normalized sediment supply as the ratio between the sediment supply and the value of $1.81\times10^8$ t, so that the maximum value of normalized sediment supply for simulation Sm1 is 1.

### 3.1 Metrics of morphology

River-dominated deltas could be categorized into digitate and lobate deltas according to their morphologic characteristics (Olariu and Bhattacharya 2006; Edmonds and Slingerland 2010). The digitate deltas are characterized by one or multiple fingers, which are elongate and separated by interdistributary bays (Fisk 1955; Donaldson 1974; Galloway 1975; Kim et al. 2009b; Rowland et al. 2010; Falcini and Jerolmack 2010). A typical example is the modern Mississippi Delta (Fisk 1955; **Fig. 6a**). In contrast, the lobate deltas develop sheet sands deposited in numerous terminal distributaries (Donaldson, 1974; Olariu and Bhattacharya, 2006), such as the Wax Delta (Dumars 2002; **Fig. 6b**). There is still not quantified definition to distinguish digitate from lobate deltas. We defined that if the most of distributaries ($\geq$ 50%) were separated by interdistributary bays, the river-dominated deltas were digitate. Otherwise, they were lobate.

**Fig. 6** Satellite maps of modern Mississippi Delta (digitate delta, a) and Wax Lake Delta (lobate delta, b). The schematic measured method of metrics is shown in **Fig. 6b**.

Besides, roughness is an important metric to characterize the shoreline morphology. Edmonds and Slingerland (2010) indicated that digitate deltas produce irregular deposits with rugose

shorelines, whereas lobate deltas produce roughly axisymmetric deposits with smooth shorelines. The shoreline roughness ($R$) is related to shoreline length ($L_{\text{Shore}}$) and area of deltaic land ($A_{\text{Land}}$) (Wolinsky et al. 2010), which is calculated as:

$$R = L_{\text{shore}} / \sqrt{A_{\text{land}}} \tag{6}$$

The shoreline is defined as the envelope line of deltaic land (an example is shown by a white dash curve in **Fig. 6b**).

## 3.2 Metrics of distributary channel

This paper differentiated distributary channels by their numbers, which included active and abandoned distributary channels. Their number was difficult to be counted in the complex distributary channel network, especially as the water discharge was high (**Fig. 4**). We defined a number flux as the number in the cross-section that is along the longshore direction and defined the average number flux as the average number in all cross-sections of a delta. The longshore direction was perpendicular to the downstream (offshore) direction, illustrated in **Fig. 6**.

We divided the distributary channels into primary and secondary distributaries, according to their differences in width and length. Primary distributaries were wide (>average width) and prograded farther downstream (>average length), like as great vessels in the body; secondary distributaries were narrow (≤average width), short (≤average length), and developed among the primary distributaries, like as capillaries in the body (**Fig. 4**).

## 3.3 Metrics of deltaic land

Deltaic land was quantified by land area, delta length, and delta width. Delta length was defined as the maximum offshore distance in a delta, and delta width was defined as the maximum longshore distance in a delta (Caldwell and Edmonds 2014; **Fig. 6b**).

# 4 Results

## 4.1 Influences of water discharge on simulated deltas

Simulated deltas with medium-grained sediment mixtures (simulations Sm1–Sm9) were taken as examples to investigate differences in the morphology, the number of distributary channels, and deltaic land under different amounts of water discharges (**Fig. 3**).

### 4.1.1 Morphologic differences

The low water discharges (as $Q \leq 1{,}600$ $m^3/s$) drove river-dominated deltas to be digitate and

most of the distributary channels were separated by interdistributary bays (simulations Sm1–Sm5, **Fig. 3**). In contrast, high river discharges (as $Q$ > 1,600 $m^3/s$) resulted in lobate deltas where distributary channels were closely spaced and deposits are sheet-like (Sm6–Sm9, **Fig. 3**). These trends were not changed when growth time or sediment supply increased (**Fig. 7**).

**Fig. 7** Growth processes of simulations Sm1 and Sm9.

Differently discharging river-dominated deltas exhibited various shoreline roughnesses (**Fig. 8**). At the same simulation time, higher water discharges resulted in more rugose shorelines than lower water discharges (**Fig. 8a**). In contrast, at the same sediment supply, differently discharging river-dominated deltas presented similar shoreline roughnesses initially; then, their shoreline roughnesses differed greatly from each other; the roughness had no obvious relationship with water discharge (**Fig. 8b**).

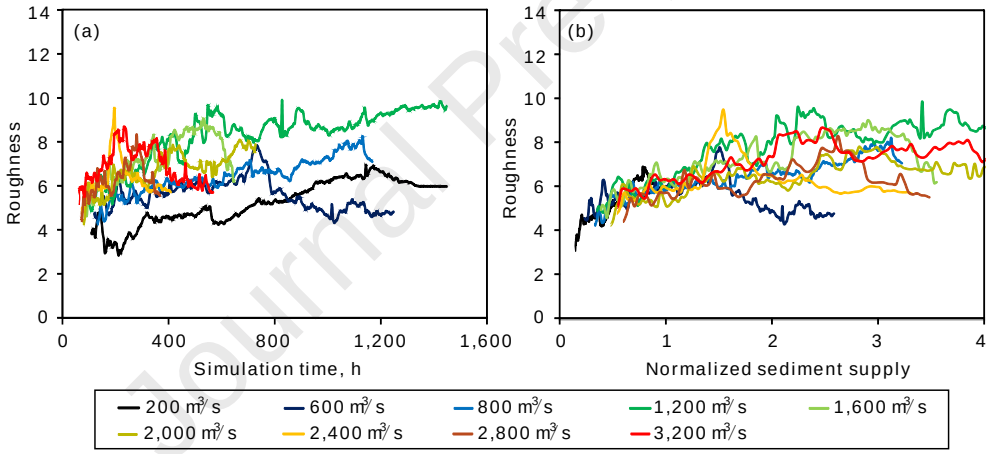


**Fig. 8** Shoreline roughnesses of simulations Sm1–Sm9. (a) Time varied roughnesses. Higher water discharges led to more rugose shorelines than lower water discharges at the same simulation time. (b) Sediment supply varied roughnesses. The shoreline roughness had no obvious relationship with water discharge at the same sediment supply.

### 4.1.2 Differences in the number of distributary channels

The number of distributary channels was positively correlated with both time-lapse and sediment supply (**Fig. 5**). Time-varied average number fluxes of distributary channels were demonstrated to logarithmically increase as the simulation advanced presenting a good correlation coefficient (such as $R^2$ = 0.98 at the water discharge of 3,200 $m^3/s$) (**Fig. 9a**). Similarly, the number of distributary channels increased as the sediment supply increases. The average number

flux of distributary channels seemed to have a logarithmic relationship with the normalized sediment supply ($R^2$ = 0.4–0.9, **Fig. 9b**). Higher water discharges led to more numbers of distributary channels than lower water discharges at the same simulation time. Taking the 320 simulation hours as an example, the average number flux of distributary channels linearly scaled with water discharge ($R^2$ = 0.88) (**Fig. 10a**). At the same sediment supply, it had no relationship with water discharge, and it was relatively stable with fluctuations when water discharge increased (**Fig. 10b**).

**Fig. 9** The number of distributary channels of simulations Sm1–Sm9. Time varied (a) and sediment supply varied (b) average number fluxes of distributary channels show that the number of distributary channels logarithmically increased as simulation advanced. Number fluxes of distributary channels at the same simulation time (c) and sediment supply (d) show that distributary channels were distributed at the more downstream locations when the water discharge was higher.

**Fig. 10** Relationships between water discharge and average number flux of distributary channels at the same simulation time (320 h) (a) and at the same normalized sediment supply (b). The average number flux of distributary channels was proportional to water discharge at the same simulation time, whereas it had a poor relationship with water discharge at the same sediment supply.

The statistical results of the number fluxes of distributary channels presented the unimodal distribution. Whether at the same simulation time or sediment supply, the peak values were higher and distributed at the further downstream locations when water discharges were higher (**Figs. 9c** and **d**). Plan views of skeletal distributary channel networks also show that higher discharges were beneficial to more numbers of distributary channels which were mostly distributed at the further downstream locations, and created more complicated distributary channel networks (**Fig. 4**).

At the low discharges, river-dominated deltas developed several primary distributaries with few secondary distributaries, such as simulations Sm1–Sm3 (**Figs. 4a–c**). In contrast, at the high discharges, river-dominated deltas developed several primary distributaries with many secondary distributaries, resulting in complicated and interlaced channel networks, such as simulations Sm8 and Sm9 (**Figs. 4h** and **i**). The number of primary distributaries in simulations Sm1–Sm9 were all less than 10. Higher discharge led to more distributary channels mainly by creating more

secondary distributaries rather than primary distributaries. However, higher discharges created wider primary distributaries because strong inertias erode banks, and they promoted primary distributaries to prograde further (**Fig. 4**). Therefore, it exited a bigger difference in the scale (width and length) between primary and secondary distributaries for river-dominated deltas with higher discharges.

### 4.1.3 Land differences

Land area increased with an increase of simulation time or sediment supply (**Figs. 11a**, **b**). At the higher discharges, river-dominated deltas built more land areas with faster building rates, compared with lower discharges. At the same simulation time, land area exhibited a positively quadratic relationship with water discharge ($R^2$ = 0.99, illustrated in **Fig. 11c**); and at the same sediment supply, the land area had a positive exponential relationship with water discharge ($R^2$ = 0.84, illustrated in **Fig. 11d**).

**Fig. 11** Land areas of simulations Sm1–Sm9. Time-varied land areas (a) and sediment supply varied land areas (b) show that deltas created more land area logarithmically as an increase of simulation time, and high discharges led to the fast land building. Relationships between land area and water discharge illustrate that land area exhibited a quadratic correlation with water discharge at the same growth time (c) and had an exponential relationship with water discharge exponential correlation at the same sediment supply (d).

The delta length and width were positively related to simulation time and sediment supply, and the increases are staircase-like due to alternate longshore and offshore progradations (**Figs. 12a–d**). River-dominated deltas prograded longshore inconspicuously as they prograded offshore, and vice versa. Therefore, higher discharging river-dominated deltas built more lands by farther offshore and longshore progradation at the same simulation time and same sediment supply, compared with smaller discharging river-dominated deltas. If one progradation period consisted of one offshore progradation period and successive longshore progradation period, delta length and width at the first progradation period were all proportional to water discharges ($R^2$ were 0.89 and 0.95, respectively; illustrated in **Figs. 12e** and **f**).

**Fig. 12** Delta lengths and widths of simulations Sm1–Sm9. Time-varied delta lengths (a) and widths

(b), sediment supply varied delta lengths (c) and widths (d) illustrate that higher discharges led to longer and wider deltas. Relationships between water discharge and delta length (e) and width (f) during the first progradation period illustrate that delta length and width were all proportional to water discharge.

## 4.2 Coupled influences of water discharge and sediment properties on simulated deltas

The simulated deltas, supplied by five kinds of sediment mixtures and steady river discharge of 1,200 $m^3$/s presented that coarse sediment mixtures (coarse-grained and low-cohesive sediments) had similar influences on river-dominated deltas to high discharges in aspects of lobate shapes, more distributary channels (**Fig. 13a**), and faster land area growth rates (**Fig. 13b**). However, coarse sediment mixtures exhibited opposite influences to high discharges in aspects of more proximal locations of distributary channels (**Fig. 13a**), smooth shorelines (**Fig. 13c**). Besides, sediment properties had fewer influences on the delta length (**Fig. 13d**).

**Fig. 13** Metric differences of river-dominated deltas with different sediment properties and same water discharge of 1200 $m^3$/s. (a) Number fluxes of distributary channels. (b) Times-varied roughness. (c) Times-varied land area. (d) Times-varied delta length.

Since both sediment properties and river discharge had significant influences on river-dominated deltas, then we analyzed the couple influences of river discharge and sediment properties. The following section focused on simulated deltas with fine-grained (Simulations Sf1–Sf9, **Fig. 14**) and coarse-grained sediment mixtures (Simulations Sc1–Sc9, **Fig. 15**), compared with simulated deltas with medium-grained sediment mixtures (Simulations Sm1–Sm9, **Fig. 3**).

**Fig. 14** Map views of water depth for simulated deltas with fine-grained sediment mixtures (Sf1–Sf9). The water discharges and simulated hours are shown in the upper-right corner.

**Fig. 15** Map views of water depth for simulated deltas with coarse-grained sediment mixtures (Sc1–Sc9). The water discharges and simulated hours are shown in the upper-right corner.

With fine-grained sediment mixtures (fine grain and high cohesion), river-dominated deltas were more digitate compared with those with medium-grained sediment mixtures (**Figs. 3** and **14**).

The higher discharges (> 2,400 $m^3/s$) also contributed to lobate shape with close-spaced distributary channels and few interdistributary bays (such as simulations Sf7and Sf9 in **Fig. 14**). At the same simulation time, higher water discharges developed more rugose shorelines and more numbers of distributary channels at further downstream locations (**Figs. 16 a–c**); at the same sediment supply, the water discharge had fewer influences on shoreline roughness and presented a slightly positive relationship with the number of distributary channels (**Figs. 16 d–f**). With fine-grained sediment mixtures, the water discharge exhibited a stronger influence on roughness, yet a weaker influence on the number of distributary channels, compared with medium-grained sediment mixtures.

**Fig. 16** Shoreline roughnesses and channel numbers of simulations Sf1–Sf9. (a) Time-varied roughnesses. (b) Number fluxes of distributary channels at the same simulation time. (c) Relationship between average number fluxes of distributary channels and water discharges at the same simulation time. (d) Sediment supply varied roughness. (e) Number fluxes of distributary channels at the same sediment supply. (f) Relationship between average number fluxes of distributary channels and water discharges at the same sediment supply.

With coarse-grained sediment mixtures, river-dominated deltas were more lobate in shape compared with deltas medium-grained sediment mixtures (**Figs. 3** and **15**). River-dominated deltas with water discharges of ≤ 800 $m^3/s$ were of digitate shape (Simulations Sc1 and Sc3 in **Fig. 15**). In contrast, the higher discharge (> 800 $m^3/s$) led river-dominated deltas to be of lobate shape with intricate distributary channel networks (Simulations Sc5–Sc9 in **Fig. 15**). Whether the simulation time or sediment supply is the same, the water discharge had similar influences on shoreline roughness and the number of distributary channels, compared with deltas with fine-grained sediment mixtures, but the water discharge had a weaker influence on roughness and a stronger influence on the number of distributary channels (**Fig. 17**).

**Fig. 17** Shoreline roughness and channel number of Simulation Sc1–Sc9. (a) Time-varied roughnesses. (b) Number fluxes of distributary channels at the same simulation time. (c) Relationship between average number fluxes of distributary channels and water discharges at the same simulation

time. (d) Sediment supply varied roughness. (e) Number fluxes of distributary channels at the same sediment supply. (f) Relationship between average number fluxes of distributary channels and water discharges at the same sediment supply.

To sum up, the effects of sediment properties and water discharge are both noticeable. Sediment properties affected the threshold values of water discharge, at which the deltas transited to be lobate from being digitate. Finer-grained sediment mixtures increased the threshold values, whereas coarse-grained sediment mixtures decreased the threshold values. Sediment properties also influenced the changing amplitude of metrics as the water discharge varied.

## 5 Discussion

We quantified the influences of water discharges on simulated river-dominated deltas, coupled with sediment properties. The following discussion focused on the examination based on modern river-dominated deltas and analyzed the coupled influence mechanism of water discharge sediment properties. Finally, this paper got some insights into the hydrocarbon exploration and land-building plan.

### 5.1 Examination based on modern river-dominated deltas

The modern river-dominated deltas widely develop in the worldwide coasts and lakes where wave and tide energies are weak. Statistical results show that 18 modern river-dominated deltas with higher average water discharges (> 1,000 $m^3/s$) are mostly lobate with sheet-like sands; in contrast, modern river-dominated deltas are mostly digitate as average water discharges are less than 1,000 $m^3/s$ (**Fig. 18**). The average water discharge presents a positive power correlation with the number of distributary channels, whereas the mud-proportion doesn't have a good relationship with the number of distributary channels, which may be due to influences of water discharges (**Fig. 18**).

**Fig. 18** Relationships between the number of distributary channels and water discharge (a) and mud proportion (b).

The adjacent river-dominated deltas formed by different branches of a supplying river could also verify the effects of water discharges. The first example is the Ganjiang River in China that split into four main branches, including the South Branch, Middle Branch, North Branch, and

West Branch. These branches finally extended into the western Poyang Lake and formed a lobate and many digitate deltas (**Fig. 2**). These river-dominated deltas consisted of similar sediment mixtures (**Table 3** and **Fig. 19**) and were developed from a similar time (~ 1,600 years ago). Poyang Lake is the biggest freshwater lake in China with an area of ~ 4,125 $km^2$, which is located in the northern Jiangxi province (**Fig. 2a**). It is an open shoal-water lake basin that has a gentle slope of < 0.1°, a shallow water depth of 8.4 m on average, and weak wave and tide energy (Jin et al. 2017). Therefore, water discharge played significant roles in these river-dominated delta growths. The Middle Branch with a higher discharge (~ 1,000 $m^3/s$) formed a big-scaled lobate delta covering more numbers of distributary channels, larger delta length and width with more land area, whereas the diversions of the South Branch, North Branch, and West Branch had much lower discharge and formed many small-scaled digitate deltas with fewer distributary channels, smaller delta length and width, and fewer land area (**Table 3** and **Fig. 2**). The lobate delta developed several primary distributaries and many secondary distributaries that are proved by the newly formed distal channels (**Fig. 17f**). And the shoreline of the lobate delta is still rugose (**Figs. 2d** and **f**). The above results match well with simulated results considering at the same simulation time.

**Fig. 19** Typical deltaic deposits of West/North Branch delta (a), Middle Branch delta (b), and South Branch delta (c), and grain size distributions (d). The deposits are mainly fine sands, which are acquired from exploratory pits.

The other example is the Mississippi River that bifurcated into three branches (Lower Mississippi River, Low Atchafalaya River Outlet, and Wax Lake Outlet). Atchafalaya River, a distributary of the Mississippi River in south-central Louisiana, carries the sediments into Atchafalaya Bay steadily, which promotes the Atchafalaya Delta and Wax Lake Delta to grow (Van Heerden 1983; Van Heerden and Roberts 1988; **Fig. 5b**). Atchafalaya Bay is located in the coastal zone in southern Louisiana, US (Evers et al. 1998) (**Fig. 5a**). The Point au Fer shell reef separates Atchafalaya Bay from the Gulf of Mexico (Fuller et al. 1984). The Atchafalaya Delta is supplied with about 70% of water discharge by the lower Atchafalaya River Outlet, and the Wax Lake Delta is supplied with only 30% of water discharge by the manmade Wax Lake Outlet (Van Heerden 1983; illustrated in **Fig. 5b**). The two river-dominated deltas deposited similar fine

sediments that consisted of fine sands, silts, and muds. They also received a similar sediment supply according to the similar depositional volume. Besides, their neighbor locations imply similar basin conditions. Then, we compare these two river-dominated deltas: (1) Atchafalaya Delta develops a similar number (~ 26) of distributary channels compared with the Wax Lake Delta (~ 25 distributary channels), with more secondary distributaries; (2) Atchafalaya Delta develops wider primary distributaries than the Wax Lake Delta; (3) Atchafalaya Delta performs a similar shoreline roughness to the Wax Lake Delta; (4) Atchafalaya Delta has a slightly larger delta length and width than the Wax Lake Delta (**Fig. 5**). These differences are more likely to be influenced by water discharge, which is a primary difference in the depositional conditions between these two deltas. The above similarities and differences match well with the simulation results considering the same sediment supply.

Atchafalaya River only brings ~ 10% of the water discharge of the Mississippi River, and most of the water discharge is taken to form Mississippi Delta, which has a much larger scale and 71 channels with a lobate shape (**Fig. 5d**). Although the Head of Passes is a typical digitate with few distributary channels, it may be affected by the facts that (1) engineered levees prevent overbank deposition and sudden changes leading to progradation of the channel into deep water area directly (**Fig. 5e**); (2) dams reduce much water discharge (Kim et al. 2009a).

## 5.2 The influence mechanism of water discharge on river-dominated deltas

Fine-grained sediment mixtures lead to digitate deltas with few distributaries because they can stabilize and thicken levees (Orton and Reading 1993; Edmonds and Slingerland 2010; Burpee et al. 2015). These levees are stronger to resist bank erosions and channel avulsions, resulting in further channel progradation, in turn, the delta perimeter receives sediment at fewer points with more rugose shoreline (Burpee et al. 2015).

Simulated and modern river-dominated deltas support that high water discharges (>1,000 $m^3/s$) are beneficial to lobate deltas, whereas low water discharges (<1,000 $m^3/s$) are beneficial to digitate deltas (**Fig. 3** and **Fig. 18a**). Some researchers also inferred that high water discharges lead to digitate deltas with long progradations (Galloway 1975; Olariu et al. 2012). We agree that high water discharge promotes the progradation, increases the width of distributary channels (especially for primary distributaries), and builds more deltaic lands faster, due to the strong inertia and sediment supply. For river-dominated deltas, compared to low water discharge, high water

discharge also leads to the lobate delta with numerous distributary channels by bifurcations and avulsions (**Fig. 7**). High water discharge favors avulsions because strong inertia is easy to erode the levee and a high Froude number is easily subject to the morphodynamic backwater effect that triggers avulsion (Hoyal and Sheets 2009; Feng et al. 2019). Edmonds and Slingerland (2007) proposed that the bifurcation length (the distance between two bifurcation points along the channel centerline) has an exponent relationship with flow velocity with an index of only 0.4. High water discharge increases bifurcation length, resulting in the decrease of bifurcation numbers at the same sediment supply, but still adds bifurcation numbers at the same growth time. Therefore, considering avulsions and bifurcations, higher water discharge promotes more numbers of distributary channels at the same growth time, yet has little influence on distributary channels at the same sediment supply (**Fig. 10**). Syvitski and Saito (2007) also showed that the number of distributary channels positively scales with water discharge, but they didn't consider the growth time and sediment supply. Besides, higher water discharge results in the wider mouth bar at the channel mouth, giving arising to sheet deposits between distributary channels (**Fig. 7**).

Although high water discharge favors the lobate delta, the deltaic shoreline is still rugose. River delta exhibits statistically isometric growth by compensational stacking (Straub et al. 2009), and deltaic deposits tend to fill in shoreline asperities and smooth the shoreline (Wolinsky et al. 2010). However, highly discharging river-dominated deltas would overfill the shoreline asperities and make the shoreline still rugose due to the over-progradation of distributary channels (**Fig. 3**).

Edmonds and Slingerland (2010) implied that the deltaic morphology is primarily controlled by sediment properties rather than water discharge. However, the number of distributary channels in modern river-dominated deltas matches well with the water discharges rather than sediment properties (**Fig. 16**). The river discharge can be larger than 10,000 $m^3/s$ such as Lena River and Mississippi River, and it can also be less than 100 $m^3/s$, such as Karatal River and diversions of the Ganjiang branches. In contrast, the critical shear stress with grain sizes > 0.01 mm is mostly < 1 $N/m^2$ (Yang and Wang 1995), which means the critical shear stress isn't common to be high like what Edmonds and Slingerland (2010) and Burpee et al. (2015) set ($\tau_{ce}(c)$ = 3.25 $N/m^2$). Levees are usually heavily colonized by plants. Although the plant was not simulated in the Delft3D models, stable plants need levees to be high enough, and it is commonly seen that modern levees with plants are avulsed by waterflood. It's reasonable to speculate that the water discharges may

even play a more important role in delta growth, compared with sediment properties. However, sediment properties affect the threshold values of water discharge. Simulations show that for fine-grained, highly-cohesive sediments, the threshold values could be more than 2,400 $m^3/s$; for coarse-grained, lowly-cohesive sediments, the threshold values could be less than 800 $m^3/s$.

Besides, the studied modern deltas in **Table 3** are mostly shallow-water deltas, if considering the Yellow River Delta and Mississippi Delta here include recent and modern deposits. Researchers proposed that the water depth is also an important factor in delta morphology (Fisk 1955; Postma 1990; Wang et al. 2019). The effect of basinal water depth on the formation of the lobate or digitate delta needs to be further studied.

Modern river-dominated deltas are mostly lobate with numerous distributary channels as water discharges are > 1,000 $m^3/s$, according to the statistical result from 18 modern river-dominated deltas. The 1,000 $m^3/s$ is a reference threshold value of water discharge, from which the deltas become lobate. Finer-grained, higher-cohesive sediments drive this threshold value to be higher, and vice versa. High basinal water depth and slope could also improve this threshold value because they favor digitate delta (Storms et al. 2007).

## 5.3 Implications for hydrocarbon exploration

In a pay zone where basinal setting (e.g. basin slope), sediment properties, sandy mouth bar thickness (related to basinal water depth) are similar, then the water discharge is an important variable. If considering similar basinal water depth, the base level changes could also indicate a variation of the water discharge. If the upstream river is a meandering river (**Fig. 16b**) so the water discharge ($Q$) can be estimated using (Schumm 1972)

$$Q = 0.028 W^{2.43} / F^{1.13} \quad (7)$$

where $W$ is the river bankfull width, m; $F$ is the width–depth ratio. A river is commonly two times wider than the corresponding distributary channels in the bar fingers, as observed from modern deposits. The water discharge is positively related to distributary channel width.

It may be helpful for the evolution analysis and inter-well prediction of river-dominated delta reservoirs to understand the effects of water discharge on river-dominated deltas. High water discharges (>1,000 $m^3/s$) are mostly lobate deltas, which develop sheet sands with high connectivity, whereas low water discharges (<1,000 $m^3/s$) are more likely to digitate deltas, which

develop bar fingers. The sandy bar fingers are separated by muddy inter-distributary bays, which present low lateral connectivity (Hu et al. 2019). For example, the digitate shallow-water deltas were developed in the Lower Member of Minghuazhen Formation, Neogene, Bohai B Oilfield, Bohai Bay Basin, China, which consisted of bar fingers in the lower delta plain-delta front (Xu et al. 2019). Their average bar fingers width was 200m and the average thickness was ~5 m (**Fig. 20**). If distributary channels approach the half-width of bar fingers, the average water discharges were less than 200 $m^3/s$, therefore, the delta morphology is digitate. The bar fingers are narrow and inter-well prediction is difficult by well data, especially in the layer IV5.1. The distributary channels in the bar fingers should also be recognized due to different sedimentary rhythms and dynamic development characteristics (Xu et al. 2019; Hu et al. 2019). The similar sand thickness of mouth bars indicates the similar basinal water depth in layers IV5.1 and IV8.2. The higher base level of layer IV5.1 indicates lower water discharge in layer IV8.2, compared to layer IV8.2, we thus predicted the narrower and fewer distributary channels, and narrower bar fingers in layer IV5.1 (**Fig. 20**).

**Fig. 20** Facies distribution of digitate deltas in the Lower Member of Minghuazhen Formation, Neogene, Bohai B Oilfield, Bohai Bay Basin, China (modified from Xu et al., 2019). (a) Layer IV5.1; (b) Layer IV8.2.

The other example is the shallow-water deltas in Chang 6–8 Formation, Huaqing Oilfield, Ordos Basin, China. The lobate shallow-water deltas were developed in Chang 6 Formation, whereas digitate shallow-water deltas were developed in Chang 8 Formation (Feng et al. 2015; Wang et al. 2019). Their sandy mouth bar thickness (~5 m) and sediment properties (fine sand–silt dominated) are similar. The water discharge was lower in Chang 8 Formation according to a higher base level, compared to Chang 6 Formation. Based on Equation (6), the water discharge is ~3,000 $m^3/s$ in Chang 6 Formation, which supports a lobate delta morphology. The distributary channel width in Chang 8 Formation is difficult to be predicted according to the well data. We consider that it was more likely to be less than 800 m, so that the water discharge could be less than 1,000 $m^3/s$. Besides, the delta width, length, and the number of distributary channels should be lower in Chang 8 Formation compared to Chang 6 Formation.

## 6 Conclusions

This paper illustrates significant influences of water discharge on the morphology, number of distributary channels, and deltaic land of river-dominated deltas, considering growth time, sediment supply, and coupled effects of sediment properties.

Simulations and modern deposits show that (1) high water discharges favor lobate deltas and low water discharges lead to digitate deltas, and the water discharge of 1,000 $m^3/s$ is a referenced threshold value at which the deltas become lobate from digitate; (2) at the same simulation time, higher water discharges lead to more rugose shorelines, more numbers of distributary channels (especially secondary distributaries), and longer and wider deltas with more land areas, whereas lower water discharges result in less shorelines rugosity and distributary channels, and shorter and narrower deltas; (3) at the same sediment supply, higher water discharges are beneficial to creation of longer and wider deltas with more land areas, yet similar shoreline roughnesses and numbers of distributary channels; (4) sediment properties affect the threshold values of water discharge; for fine-grained, highly-cohesive sediments, the threshold values could be more than 2,400 $m^3/s$; for coarse-grained, lowly-cohesive sediments, the threshold values could be less than 800 $m^3/s$. The result of this study may be helpful for inter-well prediction and vertical evolution analysis of river-dominated delta reservoirs.

## References

Baar AW, Albernaz MB, van Dijk WM, et al. Critical dependence of morphodynamic models of fluvial and tidal systems on empirical downslope sediment transport. Nat. Commun. 2019;10(1):1–12. doi:10.1038/s41467-019-12753-x.

Bagnold RA. An approach to the sediment transport problem from general physics. U. S. Geol. Survey. 1966. Prof Paper No 422–I:37.

Burpee AP, Slingerland RL, Edmonds DA, et al. Grain–size controls on the morphology and internal geometry of river–dominated deltas. J. Sediment. Res. 2015;85:699–714. doi:10.2110/jsr.2015.39.

Chalov S, Thorslund J, Kasimov N, et al. The Selenga River delta: a geochemical barrier protecting Lake Baikal waters. Regional Environmental Change. 2017;17(7):2039–53. doi: 10.1007/s10113-016-0996-1.

Chen B, Wu N, Zhou S. Experimental studies on the influence of the state flow on the diversion ratio of bifurcation river of Ganjiang River sink. Jiangxi Hydraulic Science & Technology. 2018;44(1):

33–5. (in Chinese)

Caldwell RL, Edmonds DA. The effects of sediment properties on deltaic processes and morphologies: A numerical modeling study. J. Geophys. Res. Earth Surf. 2014;119: 961–82. doi: 10.1002/2013JF002965.

Day JW, Britsch LD, Hawes SR, et al. Pattern and process of land loss in the Mississippi Delta: A spatial and temporal analysis of wetland habitat change. Estuaries. 2000;23:425–38. doi: 10.2307/1353136.

Dissanayake DMPK, Roelvink JA, Vander Wegen M. Modelled channel patterns in a schematized tidal inlet. Coastal Eng. 2009;56(11-12):1069–83. doi: 10.1016/j.coastaleng.2009.08.008.

Donaldson AC. Pennsylvanian Sedimentation of Central Appalachians. Spec. Pap. - Geol. Soc. Am. 1974;148:47–8. doi:10.1130/SPE148-p47.

Dumars AJ. Distributary mouth bar formation and channel bifurcation in the Wax Lake Delta, Atchafalaya Bay, Louisiana. Louisiana: Louisiana State University: Baton Rouge. 2002: 88 pp.

Edmonds DA, Slingerland RL. Mechanics of river mouth bar formation: Implications for the morphodynamics of delta distributary networks. J. Geophys. Res.: Earth Surf. 2007;112. doi:10.1029/2006JF000574.

Edmonds DA, Slingerland RL. Significant effect of sediment cohesion on delta morphology. Nat. Geosci. 2010;3:105–9. doi: 10.1038/ngeo730.

Edmonds DA, Slingerland RL, Best J, et al. Response of river-dominated delta channel networks to permanent changes in river discharge. Geophys. Res. Lett. 2010;37(12). doi:10.1029/2010GL043269.

Evers DE, Sasser CE, Gosselink JG, et al. The impact of vertebrate herbivores on wetland vegetation in Atchafalaya Bay, Louisiana. Estuaries. 1998;21(1):1–13. doi: 10.2307/1352543.

Fang Y, Wu C, Wang Y, et al. Lower to Middle Jurassic shallow-water delta types in the southern Junggar Basin and implications for the tectonic and climate. Sci China Technol Sc, 2016;46(07):737–56. doi: 10.1360/N092016-00172.

Feng D, Deng H, Zhou Z, et al. Paleotopographic controls on facies development in various types of braid-delta depositional systems in lacustrine basins in China. Geoscience Frontiers. 2015;6(04):579–91. doi: 10.1016/j.gsf.2014.03.007.

Feng, W, Wu, S, Zhang, K, et al. Depositional process and sedimentary model of meandering–river

shallow delta: insights from numerical simulation and modern deposition. Acta Geol. Sin. 2017;91:2047–64. (in Chinese)

Feng W, Zhang C, Yin T, et al. Sedimentary characteristics and internal architecture of a river-dominated delta controlled by autogenic process: implications from a flume tank experiment. Petroleum Science. 2019;16(2):1237-54. doi: 10.1007/s12182-019-00389-x.

Fisk HN. Sand facies of Recent Mississippi delta deposit. Italy, Rome: 4th World Petroleum Congress. 1955;377–98. doi: 10.1093/philmat/nkv020.

Falcini F, Jerolmack DJ. A potential vorticity theory for the formation of elongate channels in river deltas and lakes. J. Geophys. Res. Earth Surf. 2010;115. doi: 10.1029/2010JF001802.

Fuller DA, Sasser CE, Johnson WB, et al. The effects of herbivory on vegetation on islands in Atchafalaya bay, Louisiana. Wetlands. 1984;4(1):105–14. doi: 10.1007/BF03160490.

Galloway WE. Process framework for describing the morphologic and stratigraphic evolution of deltaic depositional systems. Deltas: Models for Exploration. Houston, Texas: Houston Geological Society. 1975:87–98.

Hoyal DCJD, Sheets BA. Morphodynamic evolution of experimental cohesive deltas. J. Geophys. Res. Earth Surf. 2009;114. doi: 10.1029/2007JF000882.

Hu Y, Huang K, Xu Z, et al. Distribution character of remaining oil with finger bar of bird-foot shoal water delta reservoir in BZ Oilfield, Bohai Bay Basin. Bulletin of Geological Science and Technology. 2019;38(2):189–98. (in Chinese)

Ikeda S. Lateral bed load transport on side slopes. J. Hydraul. Div. ASCE. 1982;108(11):1369–73. doi: 10.1061/JYCEAJ.0005937.

Jin, Z., Gao. B., Wang, J., et al. Two new types of sandbars in channels of the modern Ganjiang Delta, Poyang Lake, China: Depositional characteristics and origin. J. Palaeogeogr. 2017;6(2):132–43. doi: 10.1016/j.jop.2017.03.001.

Ji H. Sequence stratigraphy and depositional systems in the Paleogene,Liaodong Bay. Petroleum Science. 2008;52(02):110–8. doi: 10.1007/s12182-008-0018-0.

Kim W, Mohrig D, Twilley R, et al. Is it feasible to build new land in the Mississippi River delta? Eos Trans. AGU. 2009a;90:373–4. doi: 10.1029/2009EO420001.

Kim W, Dai A, Muto T, et al. Delta progradation driven by an advancing sediment source: Coupled theory and experiment describing the evolution of elongated deltas. Water Resour. Res.

2009b;45:495–512. doi:10.1029/2008WR007382.

Lesser G, Roelvink J, Van Kester J, et al. Development and validation of a three-dimensional morphological model. Coastal Eng. 2004;51:883–915. doi: 10.1016/j.coastaleng.2004.07.014.

Marciano R, Wang Z, Hibma A, et al. Modeling of channel patterns in short tidal basins. J. Geophys. Res. 2005;110. doi:10.1029/2003JF000092.

Milliman JD, Farnsworth KL. River discharge to the coastal ocean: a global synthesis. England: Cambridge University Press. 2013:200–400.

Min Q. On the regularities of water level fluctuations in Poyang Lake. J. Lake Sci. 1995;7:281–8. (in Chinese)

Morton RA, Donaldson AC. Hydrology, morphology, and sedimentology of the Guadalupe fluvial-deltaic system. GSA Bull. 1978;89(7):1030–6. doi: 10.1130/0016-7606(1978)892.0.CO;2.

Olariu C, Bhattacharya JP, Leybourne MI, et al. Interplay between river discharge and topography of the basin floor in a hyperpycnal lacustrine delta. Sedimentology. 2012;59(2):704–28. doi: 10.1111/j.1365-3091.2011.01272.x.

Olariu C, Bhattacharya JP. Terminal distributary channels and delta front architecture of river–dominated delta systems. J. Sediment. Res. 2006;76:212–33. doi: 10.2110/jsr.2006.026.

Orton GJ, Reading HG. Variability of deltaic processes in terms of sediment supply, with particular emphasis on grain size. Sedimentology. 1993;40(3): 475–512. doi: 10.1111/j.1365-3091.1993.tb01347.x.

Piliouras A, Kim W, Carlson B. Balancing aggradation and progradation on a vegetated delta: the importance of fluctuating discharge in depositional systems. J. Geophys. Res. 2017;122(10): 1882–900. doi: 10.1002/2017JF004378.

Postma, G. An analysis of the variation in delta architecture. Terra Nova. 1990;2:124–130. doi: 10.1111/j.1365-3121.1990.tb00052.x.

Propastin P. Problems of water resources management in the drainage basin of Lake Balkhash with respect to political development. In Climate change and the sustainable use of water resources. Berlin: Springer. 2012:449–61.

Rowland JC, Dietrich WE, Stacey MT. Morphodynamics of subaqueous levee formation: Insights into river mouth morphologies arising from experiments. J. Geophys. Res. Earth Surf. 2010;115. doi: 10.1029/2010JF001684.

Schumm SA. Fluvial paleochannels. Soc. Econ. Paleontol. Mineral. 1972;SP16:98–107.

Shaw JB, Wolinsky MA, Paola C, et al. An image- based method for shoreline mapping on complex coasts. Geophys. Res. Lett. 2008;35. doi: 10.1029/2008GL033963.

Shankman D, Keim BD, Song J. Flood frequency in China's Poyang Lake region: trends and teleconnections. Int. J. Climatol. 2006;26(9): 1255–66. doi: 10.1002/joc.1307.

Straub KM, Paola C, Mohrig D, et al. Compensational stacking of channelized sedimentary deposits. J. Sediment. Res. 2009;79:673–88. doi:10.2110/jsr.2009.070.

Storms JEA, Stive MJF, Roelvink DA, et al. Initial morphologic and stratigraphic delta evolution related to buoyant river plumes. Coastal Sediments. 2007;07:736–48. doi: 10.1061/40926(239)56

Syvitski JPM., Kettner AJ, Overeem I, et al. Sinking deltas due to human activities, Nat. Geosci. 2009;2: 681–6. doi: 10.1038/ngeo629.

Syvitski JP, Saito Y. Morphodynamics of deltas under the influence of humans. Global and Planetary Change. 2007;57(3-4):261–82. doi: 10.1016/j.gloplacha.2006.12.001.

Tejedor A, Longjas A, Caldwell R, et al. Quantifying the signature of sediment composition on the topologic and dynamic complexity of river delta channel networks and inferences toward delta classification. Geophys. Res. Lett. 2016;43:3280–7. doi: 10.1002/2016GL068210.

Tejedor A, Longjas A, Zaliapin I, et al. Delta channel networks: 2. Metrics of topologic and dynamic complexity for delta comparison, physical inference, and vulnerability assessment. Water Resour. Res. 2015;51(6):4019–45. doi: 10.1002/2014WR016604.

Törnqvist TE, Wallace DJ, Storms JEA, et al. Mississippi Delta subsidence primarily caused by compaction of Holocene strata. Nat. Geosci. 2008;1:173–6. doi: 10.1038/ngeo129.

Van Heerden IL. Deltaic sedimentation in eastern Atchafalaya Bay. Louisiana. Louisiana: Louisiana State University: Baton Rouge. 1983:117.

Van Heerden IL, Roberts HH. Facies development of Atchafalaya Delta, Louisiana: a modern bayhead delta. AAPG Bull. 1988;72(4):439–53. doi: 10.1306/703C8EB1-1707-11D7-8645000102C1865D.

Van Rijn LC. Principles of sediment transport in rivers, estuaries and coastal seas. Amsterdam: Aqua publications. 1993:10–50.

Vörösmarty CJ, Syvitski J, Day J, et al. Battling to save the world's river deltas. Bull. At. Sci. 2009;65(2):31–43. doi: 10.2968/065002005.

Wang J, Muto T, Urata K, Sato T, et al. Morphodynamics of river deltas in response to different basin

water depths: an experimental examination of the grade index model. Geophys. Res. Lett. 2019;46(10):5265–73. doi:10.1029/2019GL082483.

Wang T, Deng X, Wu S, et al. Differential distribution mechanism of tight sandstone oil by the reservoir properties in scale of single layer: A case of the Chang 81 reservoirs in Yanchang Formation, Huaqing Area, Ordos Basin. Journal of Northwest University (Natural Science Edition). 2019;49(3):395–405. (in Chinese)

Wang Y, Storms JEA, Martinius AW, et al. Evaluating alluvial stratigraphic response to cyclic and non-cyclic upstream forcing through process-based alluvial architecture modelling. Basin Res. 2020;33(1):48–65. doi: 10.1111/bre.12454.

Wang Z, Liang Z. Dynamic characteristics of the Yellow River mouth. Earth Surf. Processes Landforms. 2000;25(7):765–82. doi: 10.1002/1096-9837(200007)25:73.0.CO;2-K.

Wolinsky MA, Edmonds DA, Martin J, et al. Delta allometry: Growth laws for river deltas. Geophys. Res. Lett. 2010;37(21). doi: 10.1029/2010GL044592.

Woodroffe CD, Nicholls RJ, Saito Y, et al. Landscape variability and the response of Asian megadeltas to environmental change. Global Change and Integrated Coastal Management. Berlin: Springer. 2006;10:277–314. doi:10.1007/1-4020-3628-0_10.

Xu Z, Wu S, Liu Z, et al. Sandbody architecture of the bar finger within shoal water delta front: Insights from the Lower Member of Minghuazhen Formation, Neogene, Bohai BZ25 Oilfield, Bohai Bay Basin, East China. Petroleum Exploration and Development. 2019;46:1–12. doi: CNKI:SUN:PEAD.0.2019-02-013.

Yang M, Wang G. The incipient motion formulas for cohesive fine sediments. J. Bas. Sci. Eng. 1995;3:99–109. (in Chinese)

Yu Y, Lin L, Gao J, et al. Formation mechanisms and sequence response of authigenic grain-coating chlorite: evidence from the Upper Triassic Xujiahe Formation in the southern Sichuan Basin, China. Petroleum Science. 2016;13:657–68. doi:10.1007/s12182-016-0125-2.

Yuan L, Liu Y, Qiao G. Impacts of significant reduction of sediment flux into the sea in Luanhe River estuary on wetland ecological environment. South-to-North Water Diversion and Water Sci. Technol. 2011;9(04):109–12+16. doi: 10.1002/clc.20818. (in Chinese)

Zeng H, Zhao X, Zhu X, et al. Seismic sedimentology of sub-clinoformal shallow-water meandering river delta: A case from the Suning area of Raoyang sag in Jizhong Depression, Bohai Bay Basin,

NE China. Petrol Explor Dev. 2015;42(5):621–32. doi: org/10.1016/S1876-3804(15)30057-4.

Zhang L, Bao Z, Lin Y, et al. Genetic types and sedimentary model of sandbodies in a shallow-water delta: A case study of the first Member of Cretaceous Yaojia Formation in Qian'an area, south of Songliao Basin, NE China. Petrol Explor Dev. 2017;44(5):770–9. doi: 10.1016/S1876-3804(17)30087-3.

Zhang Q, Zhu X, Steel RJ, Zhong D. Variation and mechanisms of clastic reservoir quality in the Paleogene Shahejie Formation of the Dongying Sag, Bohai Bay Basin, China. Pet. Sci. 2014;11(2):200–10. doi: 10.1007/s12182-014-0333-6.

Zou C, Zhang X, Luo P, et al. Shallow-lacustrine sand-rich deltaic depositional cycles and sequence stratigraphy of the Upper Triassic Yanchang Formation, Ordos Basin, China. Basin Res. 2010;22:108–25. doi: 10.1111/j.1365-2117.2009.00450.x.

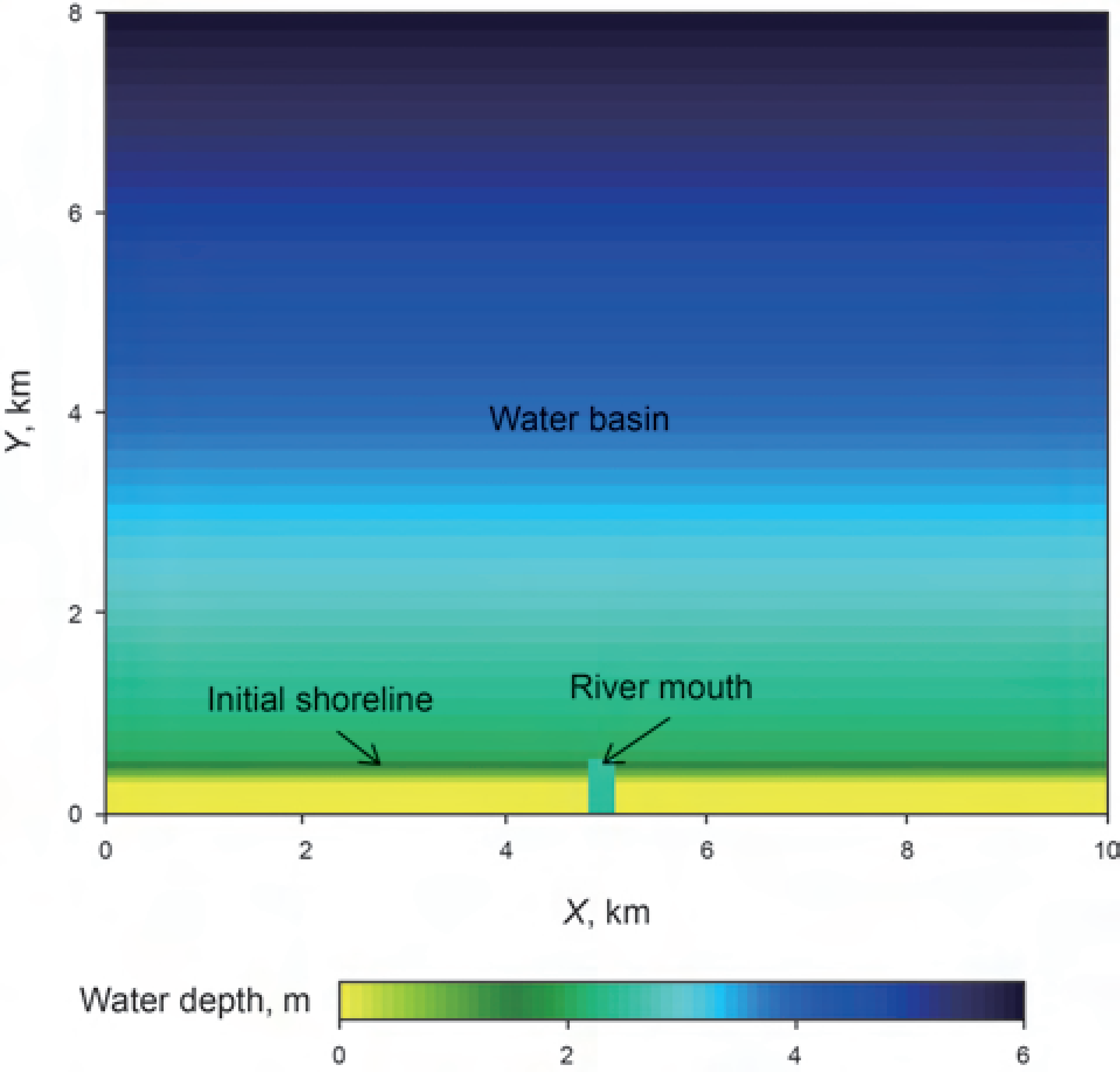
Water basin
Initial shoreline
River mouth
Y, km
X, km
0
2
4
6
8
10
Water depth, m
0
2
4
6

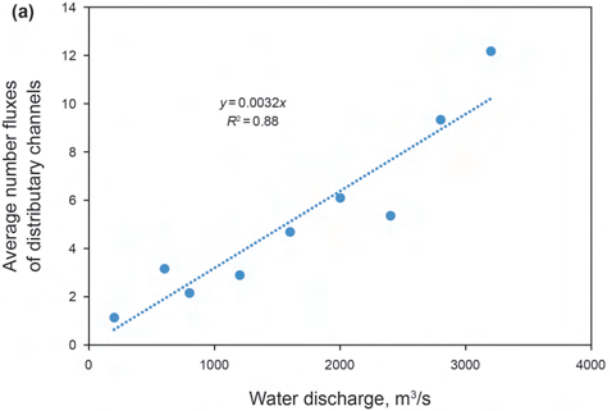
(a)
Average number fluxes of distributary channels
y = 0.0032x
R² = 0.88
Water discharge, m³/s
0
2
4
6
8
10
12
14
1000
2000
3000
4000

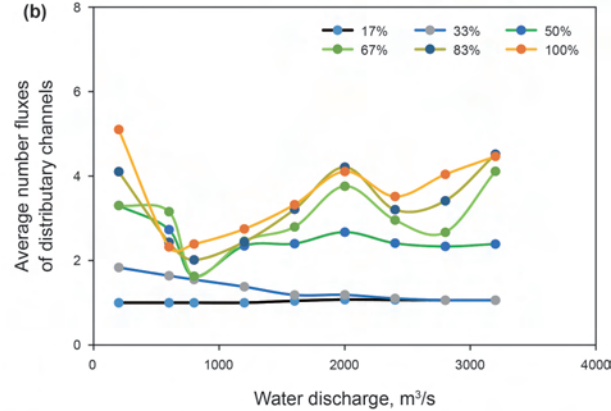
(b)
17%
33%
50%
67%
83%
100%
Average number fluxes of distributary channels
Water discharge, m³/s
0
2
4
6
8
1000
2000
3000
4000

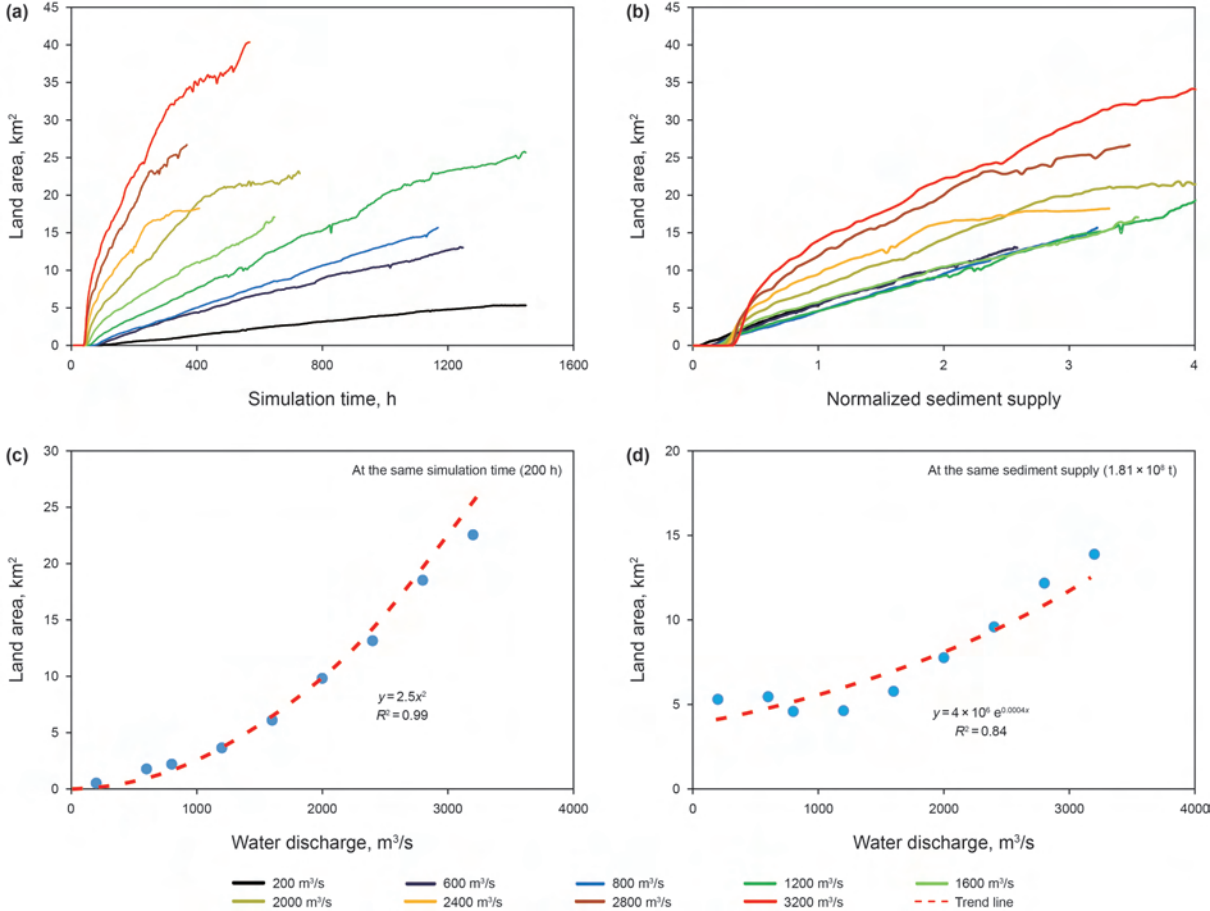
(a)
Land area, km²
Simulation time, h
(b)
Land area, km²
Normalized sediment supply
(c)
At the same simulation time (200 h)
Land area, km²
y = 2.5x²
R² = 0.99
Water discharge, m³/s
(d)
At the same sediment supply (1.81 × 10⁸ t)
Land area, km²
y = 4 × 10⁶ e^0.0004x
R² = 0.84
Water discharge, m³/s
200 m³/s
600 m³/s
800 m³/s
1200 m³/s
1600 m³/s
2000 m³/s
2400 m³/s
2800 m³/s
3200 m³/s
Trend line

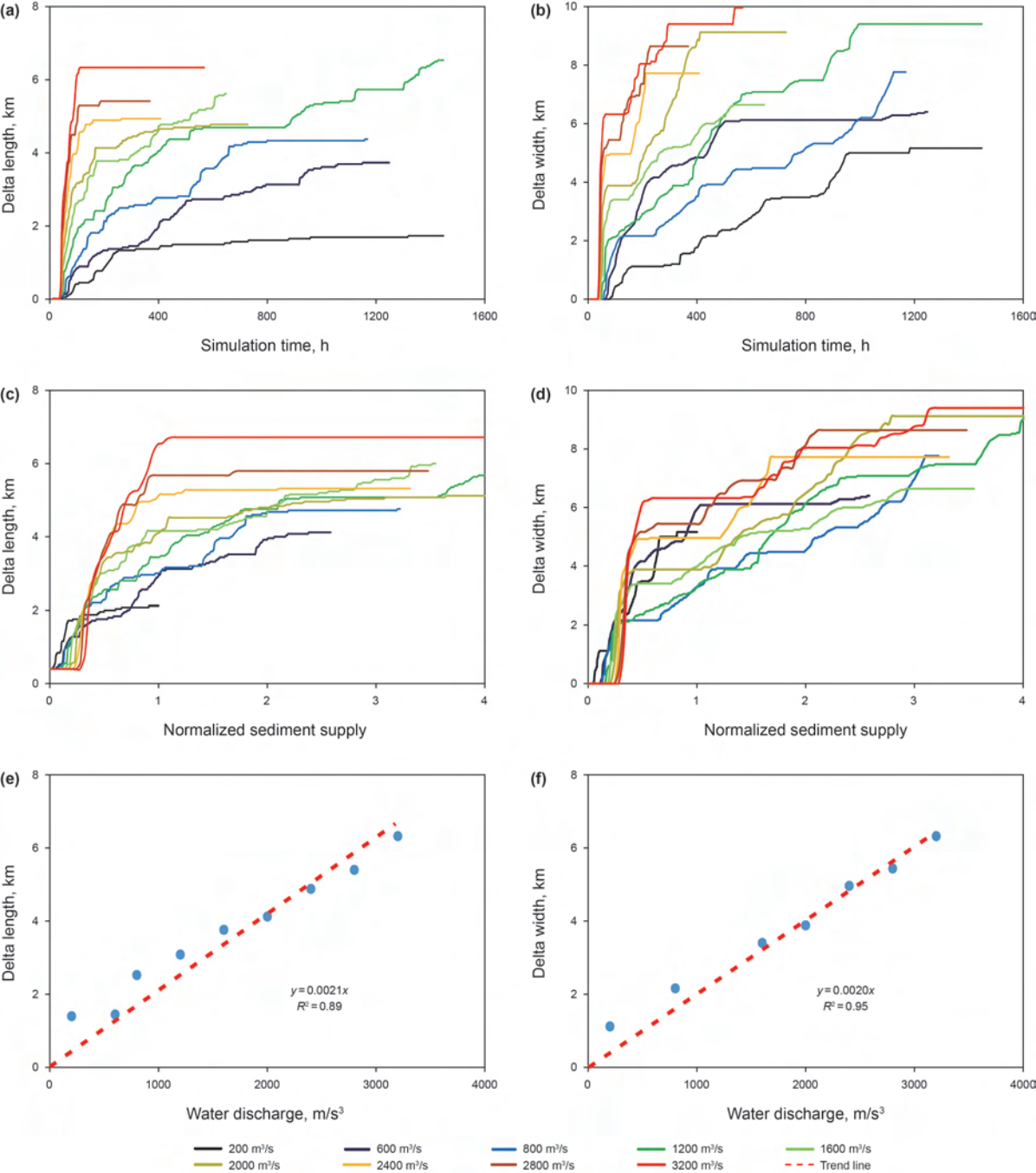
(a)
Delta length, km
Simulation time, h
(b)
Delta width, km
Simulation time, h
(c)
Delta length, km
Normalized sediment supply
(d)
Delta width, km
Normalized sediment supply
(e)
Delta length, km
y = 0.0021x
R² = 0.89
Water discharge, m/s³
(f)
Delta width, km
y = 0.0020x
R² = 0.95
Water discharge, m/s³
200 m³/s
600 m³/s
800 m³/s
1200 m³/s
1600 m³/s
2000 m³/s
2400 m³/s
2800 m³/s
3200 m³/s
Trend line

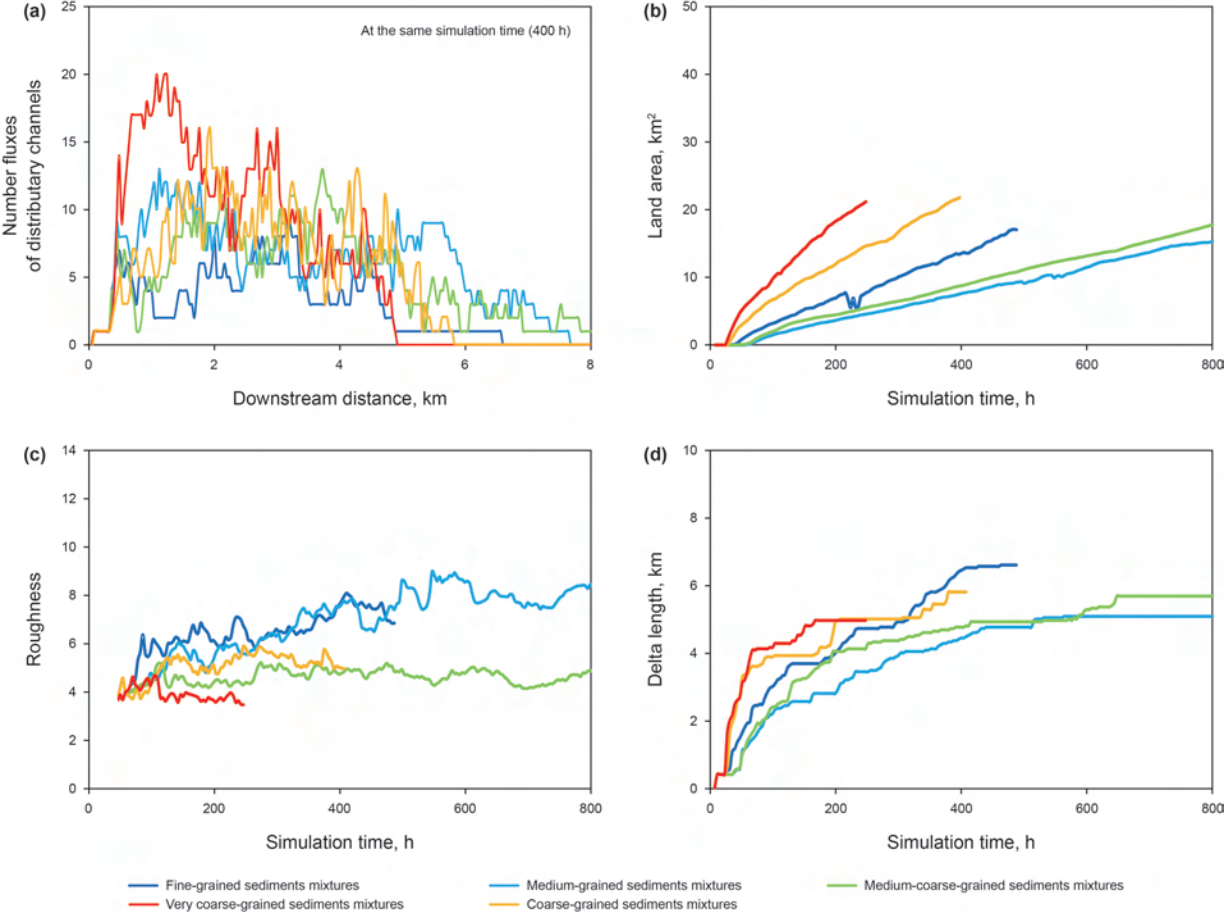
(a)
At the same simulation time (400 h)
Number fluxes of distributary channels
Downstream distance, km
(b)
Land area, km²
Simulation time, h
(c)
Roughness
Simulation time, h
(d)
Delta length, km
Simulation time, h
Fine-grained sediments mixtures
Very coarse-grained sediments mixtures
Medium-grained sediments mixtures
Coarse-grained sediments mixtures
Medium-coarse-grained sediments mixtures

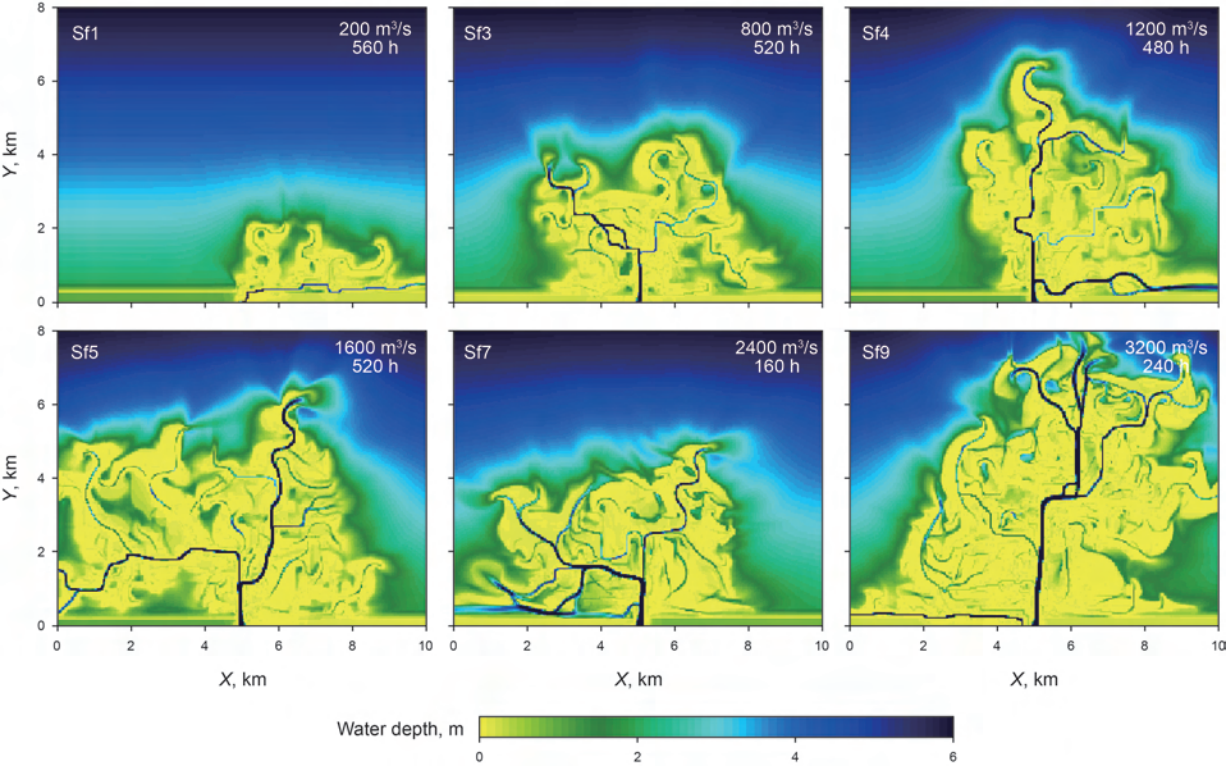
Sf1
200 m³/s
560 h
Sf3
800 m³/s
520 h
Sf4
1200 m³/s
480 h
Sf5
1600 m³/s
520 h
Sf7
2400 m³/s
160 h
Sf9
3200 m³/s
240 h
Y, km
X, km
Water depth, m
0
2
4
6
8
10

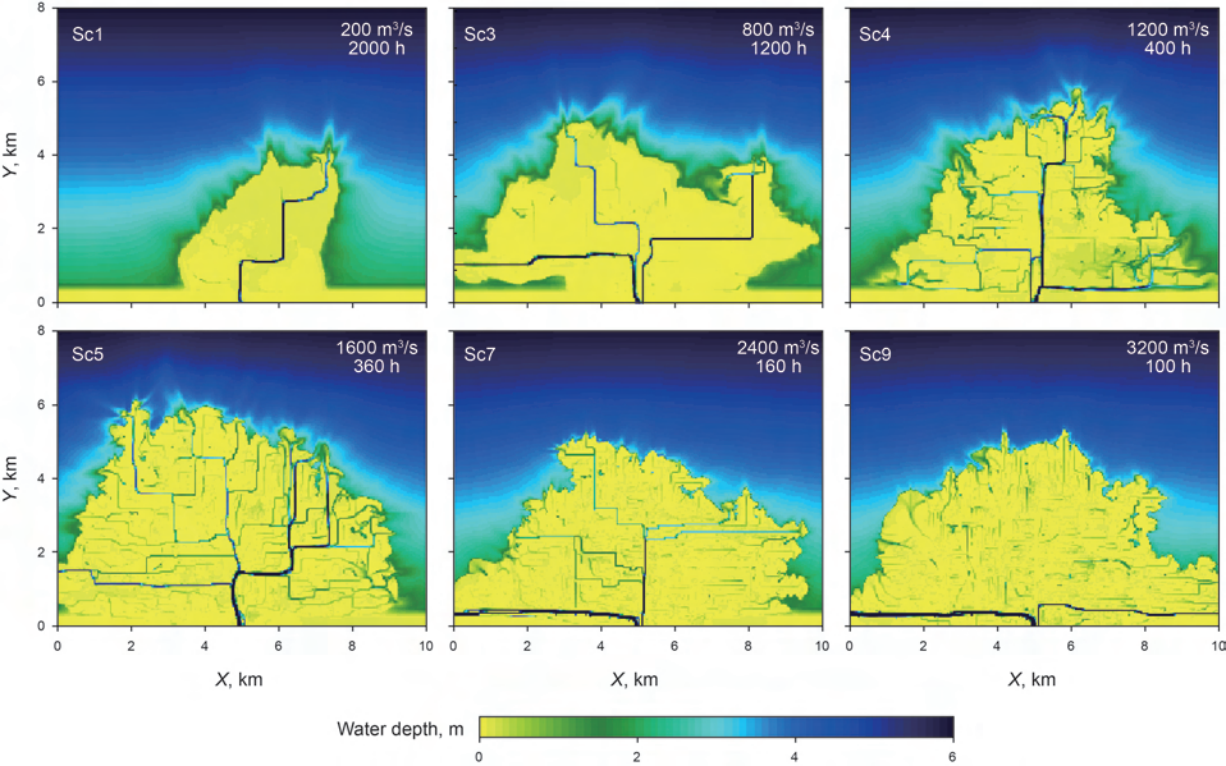
Sc1
200 m³/s
2000 h
Sc3
800 m³/s
1200 h
Sc4
1200 m³/s
400 h
Sc5
1600 m³/s
360 h
Sc7
2400 m³/s
160 h
Sc9
3200 m³/s
100 h
Y, km
X, km
Water depth, m
0
2
4
6
8
10

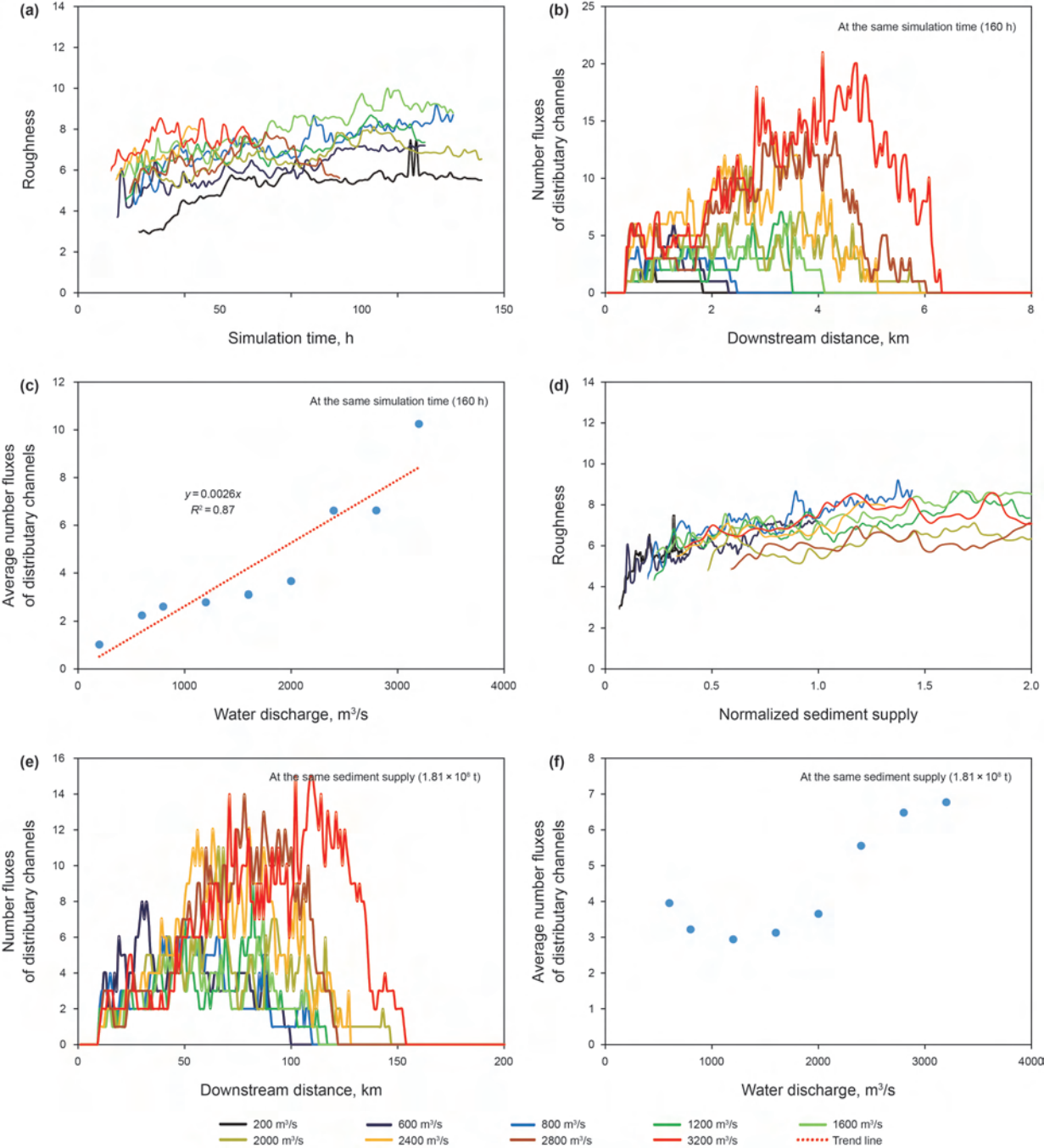
(a)
Roughness
Simulation time, h
(b)
At the same simulation time (160 h)
Number fluxes of distributary channels
Downstream distance, km
(c)
At the same simulation time (160 h)
y = 0.0026x
R² = 0.87
Average number fluxes of distributary channels
Water discharge, m³/s
(d)
Roughness
Normalized sediment supply
(e)
At the same sediment supply (1.81 × 10⁸ t)
Number fluxes of distributary channels
Downstream distance, km
(f)
At the same sediment supply (1.81 × 10⁸ t)
Average number fluxes of distributary channels
Water discharge, m³/s
200 m³/s
600 m³/s
800 m³/s
1200 m³/s
1600 m³/s
2000 m³/s
2400 m³/s
2800 m³/s
3200 m³/s
Trend line

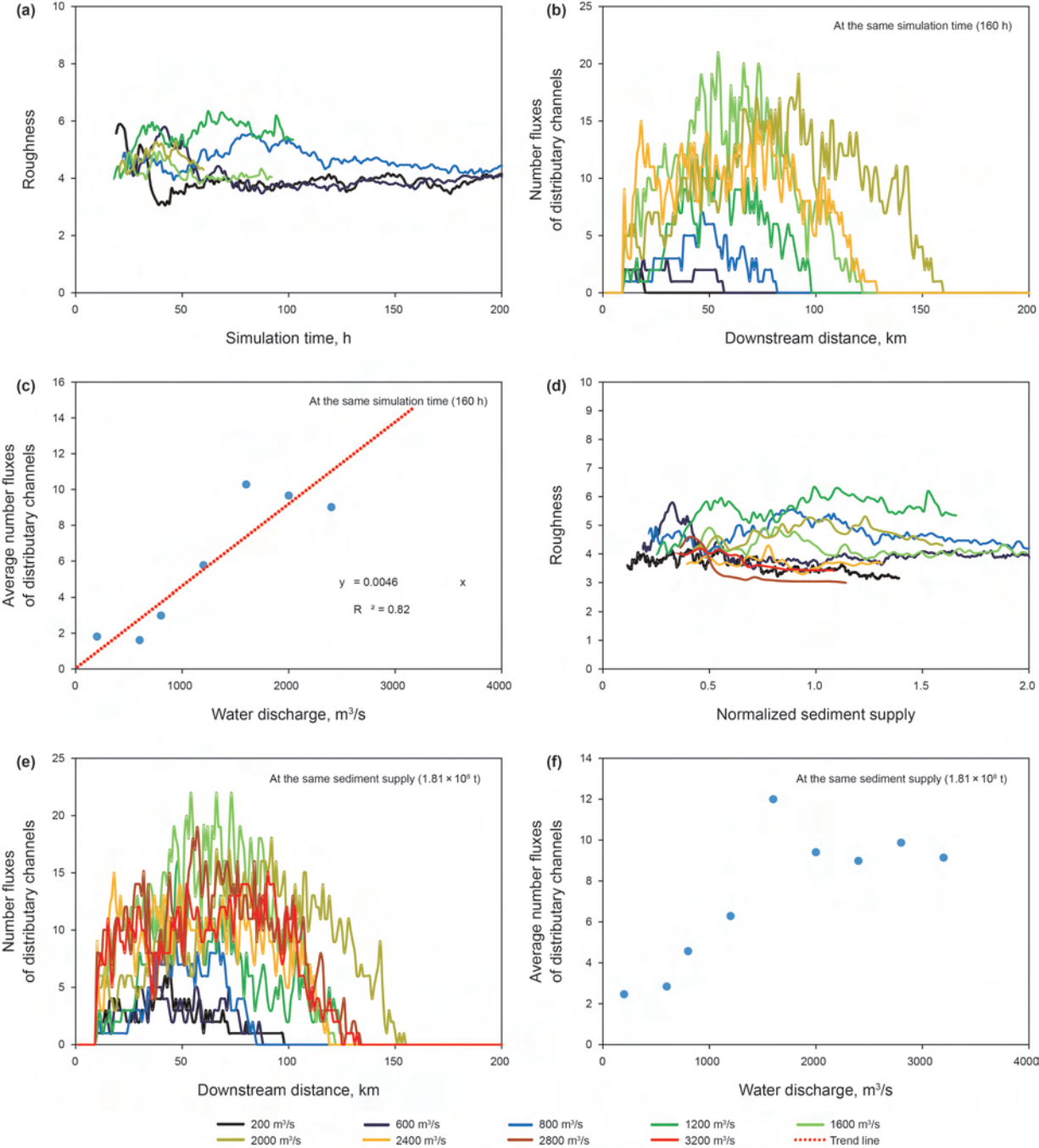
(a)
Roughness
Simulation time, h
(b)
At the same simulation time (160 h)
Number fluxes of distributary channels
Downstream distance, km
(c)
At the same simulation time (160 h)
Average number fluxes of distributary channels
y = 0.0046 x
R ² = 0.82
Water discharge, m³/s
(d)
Roughness
Normalized sediment supply
(e)
At the same sediment supply (1.81 × 10⁸ t)
Number fluxes of distributary channels
Downstream distance, km
(f)
At the same sediment supply (1.81 × 10⁸ t)
Average number fluxes of distributary channels
Water discharge, m³/s
200 m³/s
600 m³/s
800 m³/s
1200 m³/s
1600 m³/s
2000 m³/s
2400 m³/s
2800 m³/s
3200 m³/s
Trend line

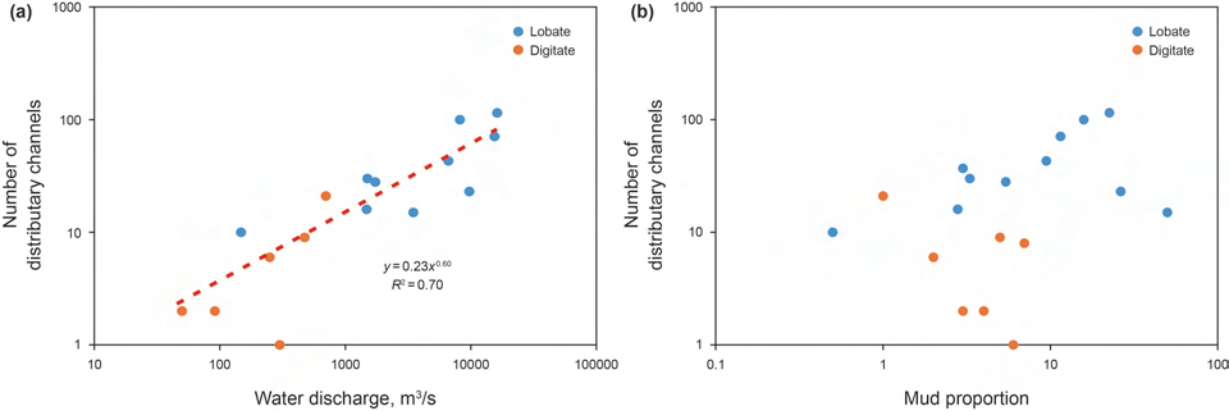
(a)
Lobate
Digitate
Number of distributary channels
1000
100
10
1
10
100
1000
10000
100000
$y = 0.23x^{0.60}$
$R^2 = 0.70$
Water discharge, m³/s
(b)
Lobate
Digitate
Number of distributary channels
1000
100
10
1
0.1
1
10
100
Mud proportion


(a)
10 cm


(b)
10 cm


(c)
cm

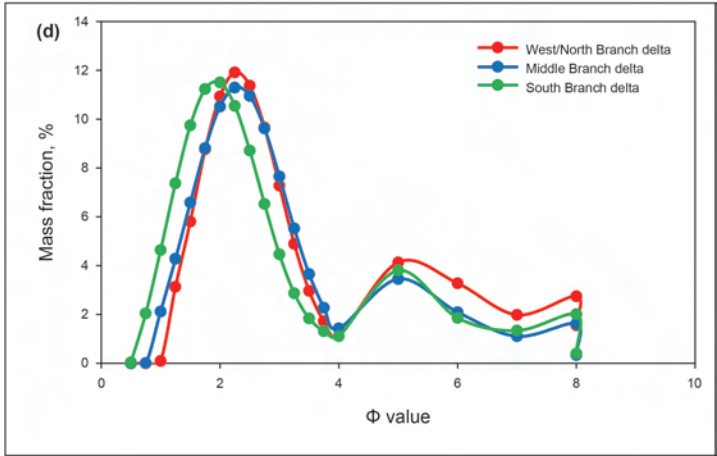
(d)
West/North Branch delta
Middle Branch delta
South Branch delta
Mass fraction, %
Φ value
0
2
4
6
8
10
12
14

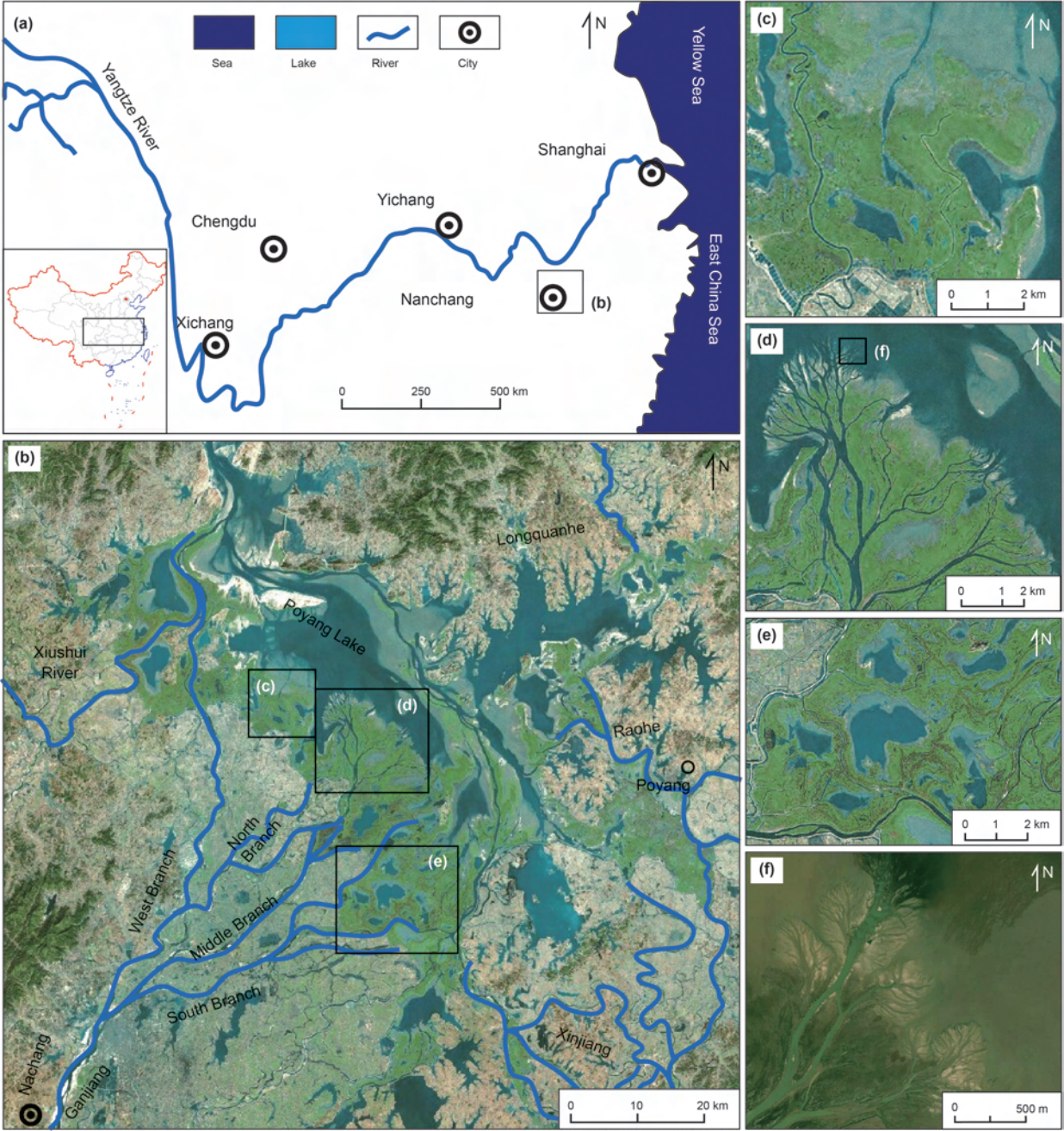
(a)
Sea
Lake
River
City
N
Yangtze River
Yellow Sea
East China Sea
Shanghai
Yichang
Chengdu
Nanchang
(b)
Xichang
0 250 500 km
(b)
Longquanhe
Poyang Lake
Xiushui River
(c)
(d)
Raohe
Poyang
North Branch
West Branch
Middle Branch
South Branch
(e)
Xinjiang
Nachang
Ganjiang
0 10 20 km
(c)
0 1 2 km
(d)
(f)
0 1 2 km
(e)
0 1 2 km
(f)
0 500 m

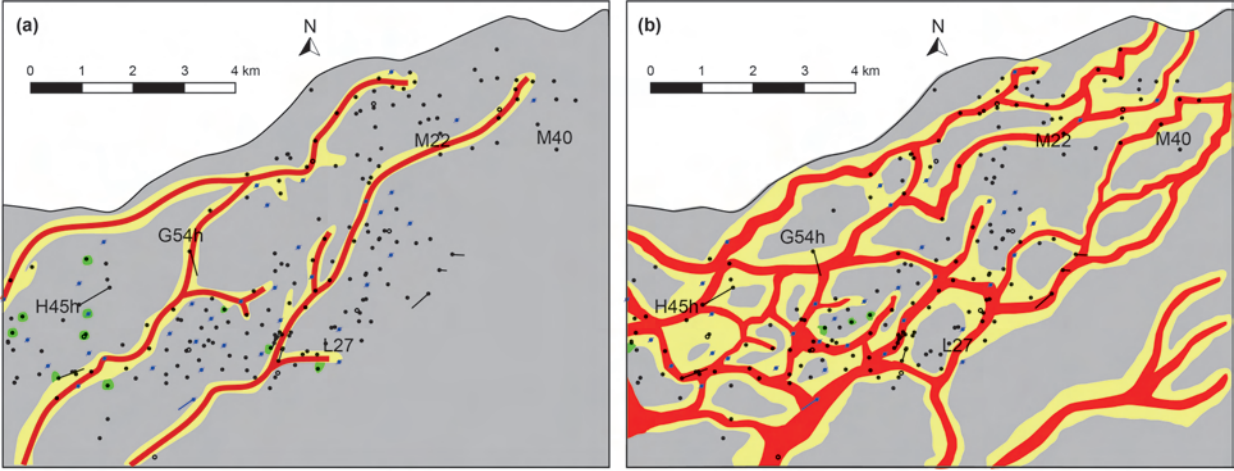
(a)
N
0 1 2 3 4 km
M22
M40
G54h
H45h
L27
(b)
N
0 1 2 3 4 km
M22
M40
G54h
H45h
L27
Distributary channel
Mouth bar
Overbank
Inter-distributary bay
Production well
Proposed well
Injection well

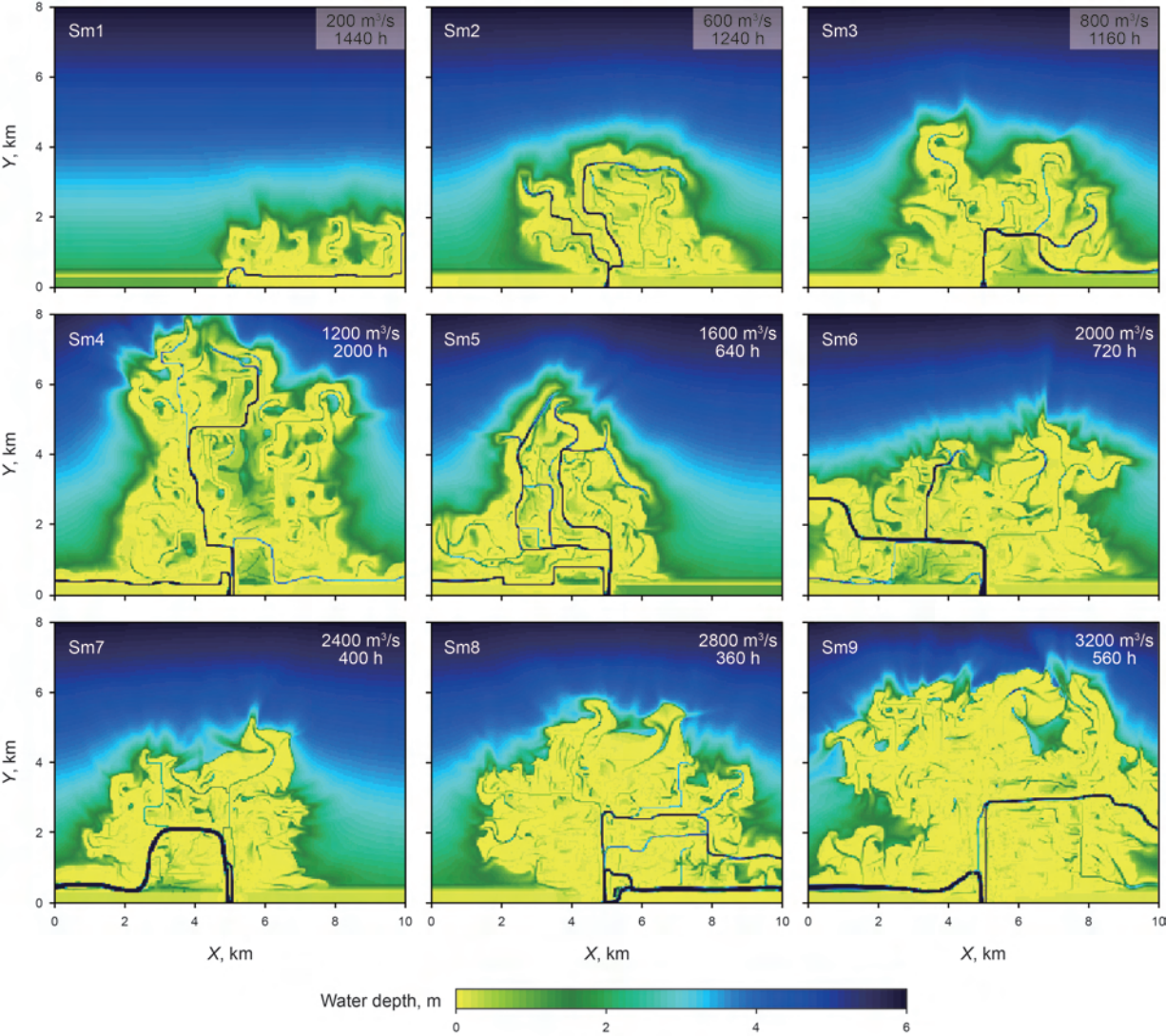
Sm1
200 m³/s
1440 h
Sm2
600 m³/s
1240 h
Sm3
800 m³/s
1160 h
Sm4
1200 m³/s
2000 h
Sm5
1600 m³/s
640 h
Sm6
2000 m³/s
720 h
Sm7
2400 m³/s
400 h
Sm8
2800 m³/s
360 h
Sm9
3200 m³/s
560 h
Y, km
X, km
0
2
4
6
8
10
Water depth, m
0
2
4
6

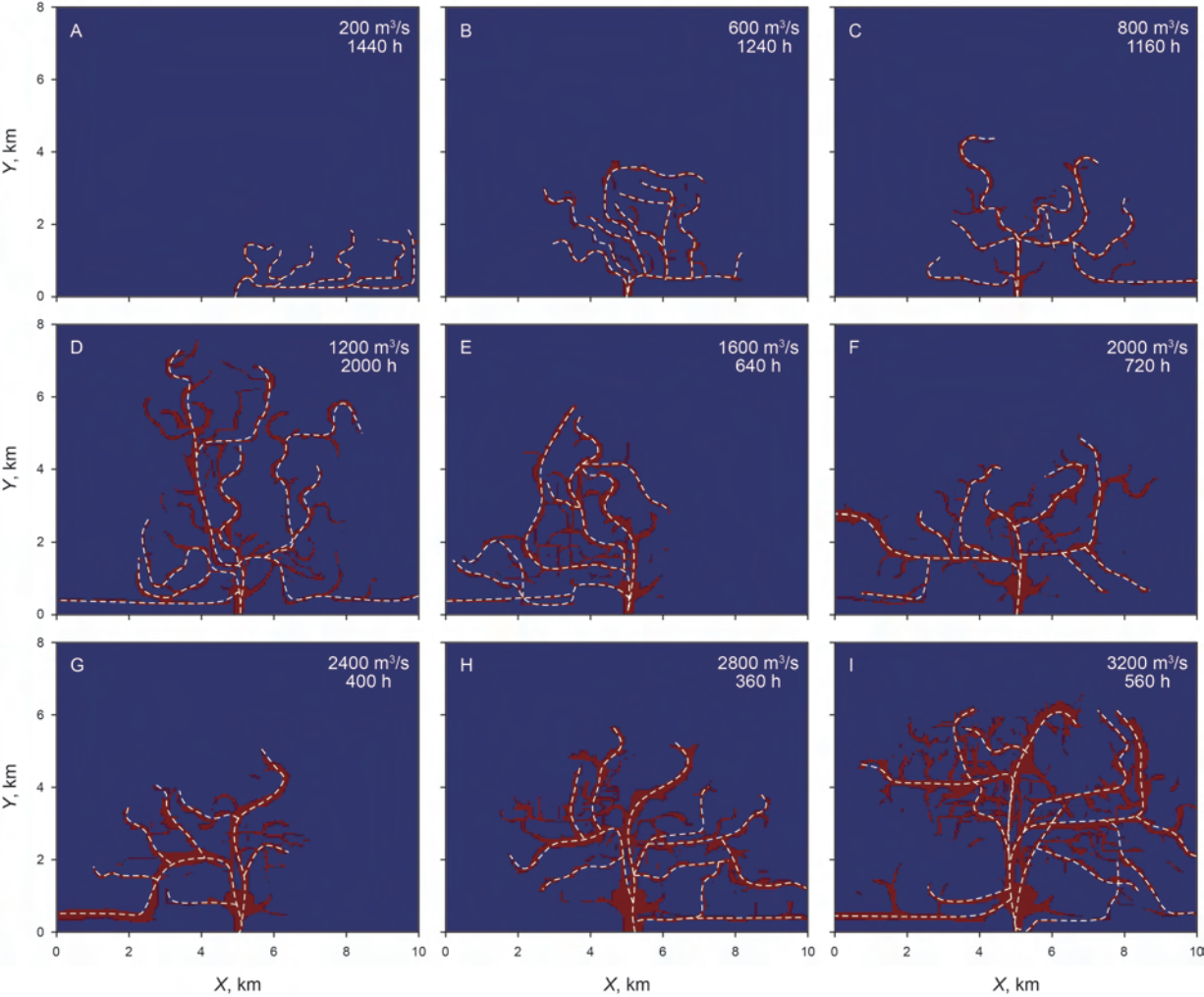
A
200 m3/s
1440 h
B
600 m3/s
1240 h
C
800 m3/s
1160 h
D
1200 m3/s
2000 h
E
1600 m3/s
640 h
F
2000 m3/s
720 h
G
2400 m3/s
400 h
H
2800 m3/s
360 h
I
3200 m3/s
560 h
Y, km
X, km
0
2
4
6
8
10

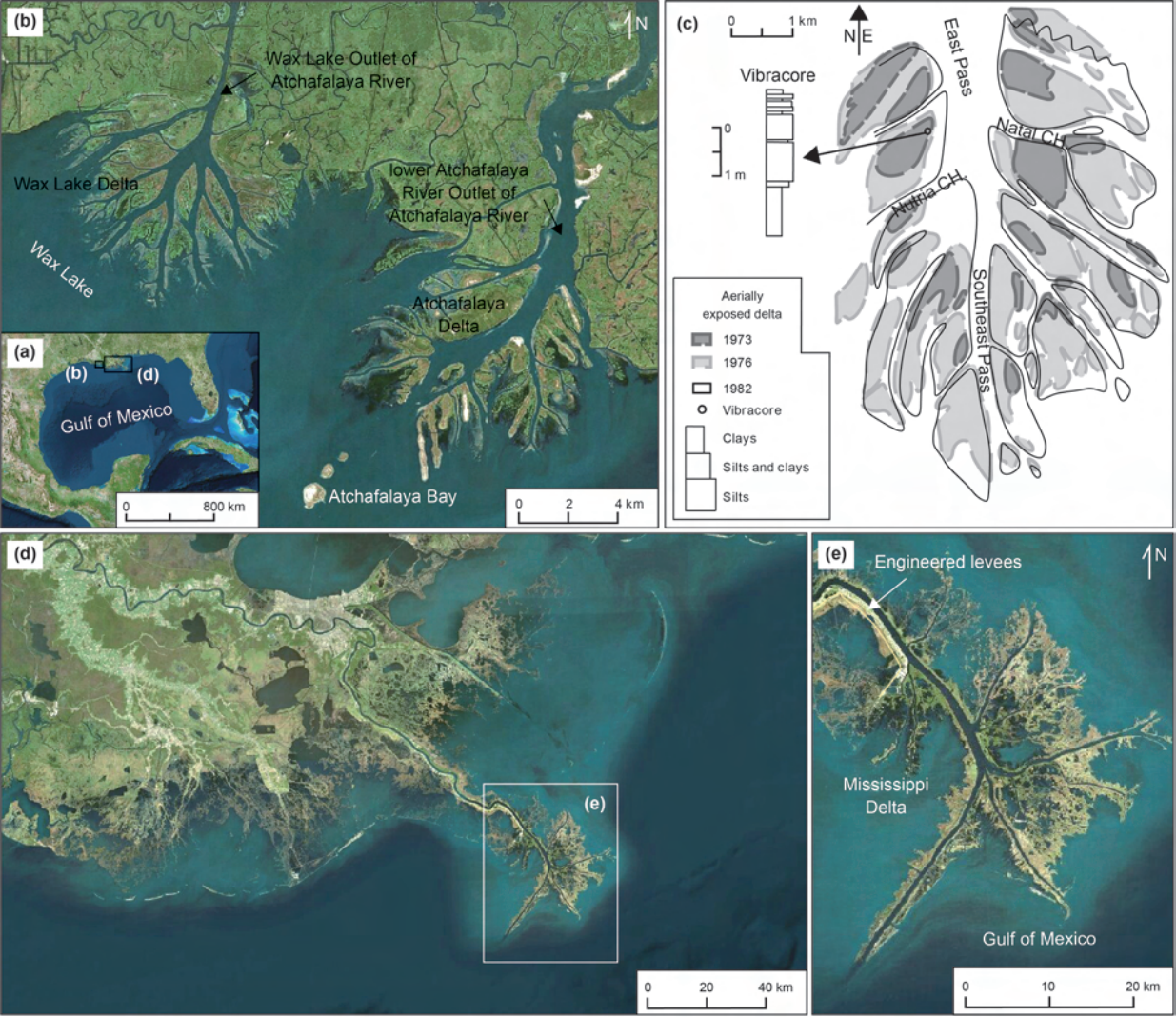
(b)
Wax Lake Outlet of Atchafalaya River
Wax Lake Delta
Lower Atchafalaya River Outlet of Atchafalaya River
Wax Lake
Atchafalaya Delta
Atchafalaya Bay
N
0 2 4 km
(a)
(b)
(d)
Gulf of Mexico
0 800 km
(c)
0 1 km
N E
Vibracore
0
1 m
East Pass
Natal CH
Nutria CH
Southeast Pass
Aerially exposed delta
1973
1976
1982
Vibracore
Clays
Silts and clays
Silts
(d)
(e)
0 20 40 km
(e)
Engineered levees
N
Mississippi Delta
Gulf of Mexico
0 10 20 km

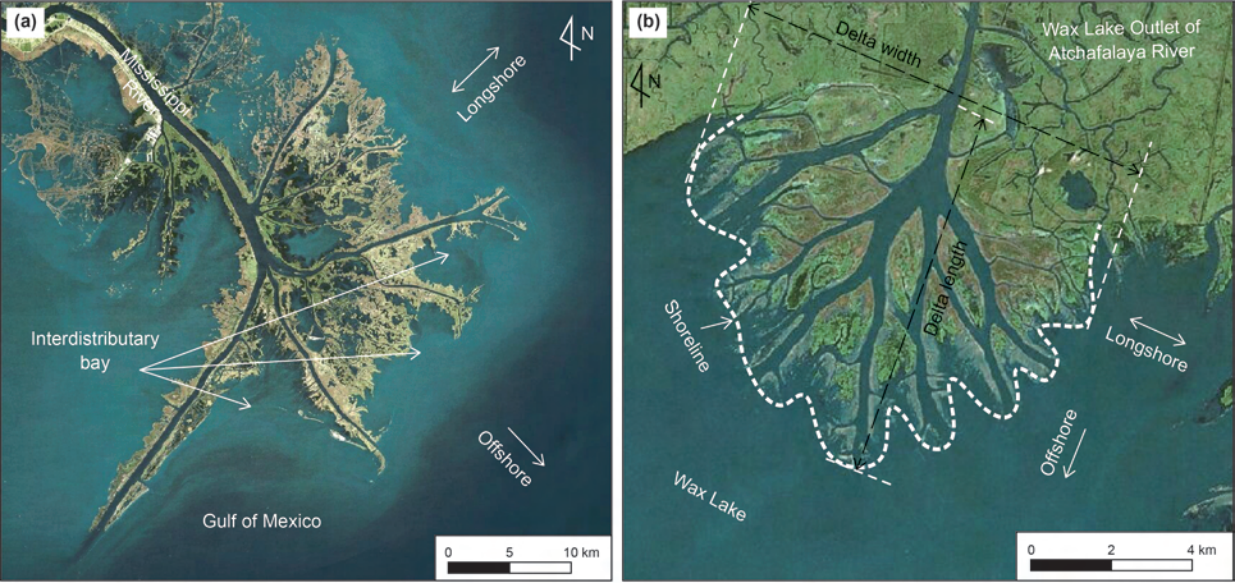
(a)
Mississippi River
Longshore
N
Interdistributary bay
Offshore
Gulf of Mexico
0
5
10 km
(b)
Wax Lake Outlet of Atchafalaya River
Delta width
N
Shoreline
Delta length
Longshore
Offshore
Wax Lake
0
2
4 km

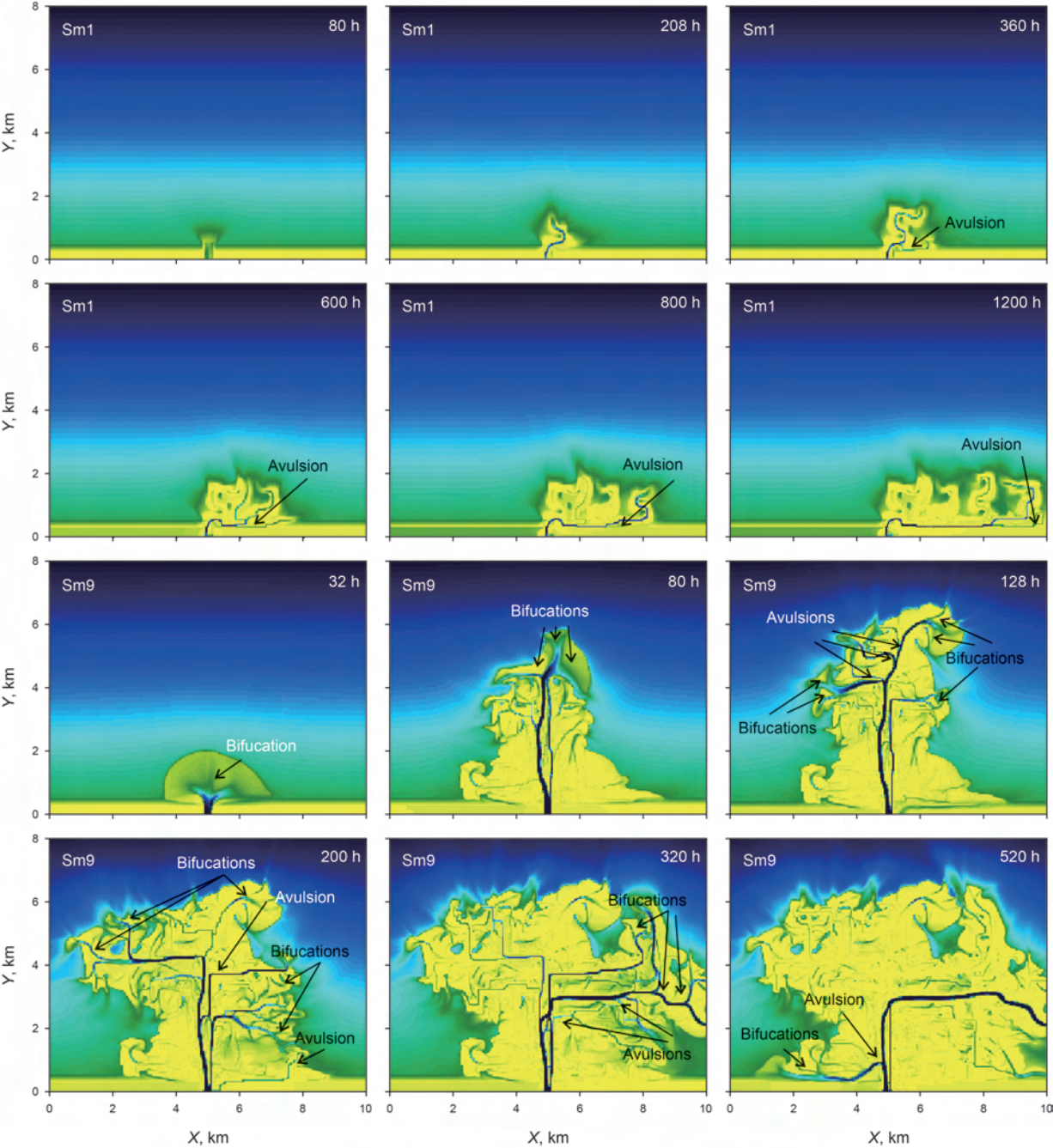
Sm1
80 h
Sm1
208 h
Sm1
360 h
Avulsion
Sm1
600 h
Avulsion
Sm1
800 h
Avulsion
Sm1
1200 h
Avulsion
Sm9
32 h
Bifucation
Sm9
80 h
Bifucations
Sm9
128 h
Avulsions
Bifucations
Bifucations
Sm9
200 h
Bifucations
Avulsion
Bifucations
Avulsion
Sm9
320 h
Bifucations
Avulsions
Sm9
520 h
Avulsion
Bifucations
Y, km
X, km
Water depth, m
0
2
4
6

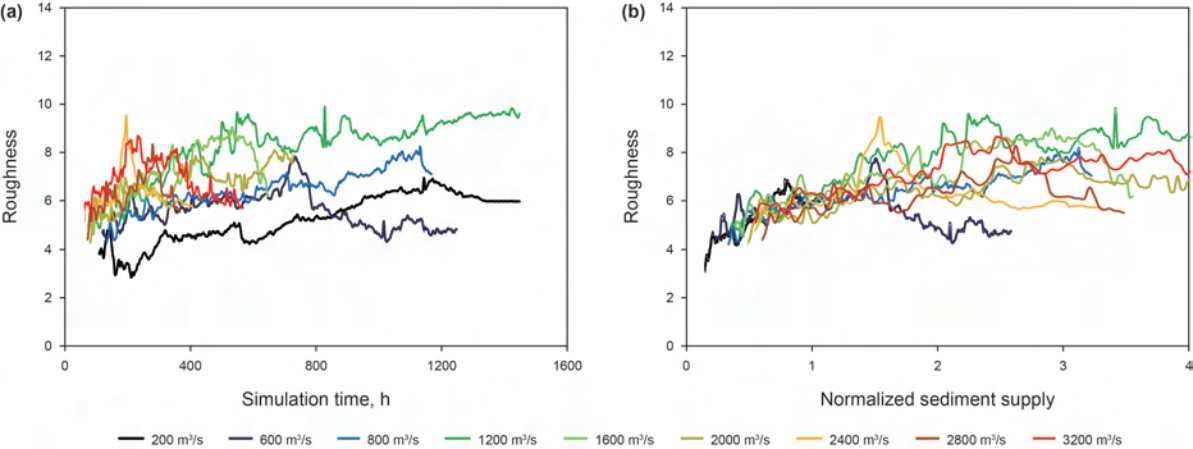
(a)
Roughness
Simulation time, h
(b)
Roughness
Normalized sediment supply
200 m³/s
600 m³/s
800 m³/s
1200 m³/s
1600 m³/s
2000 m³/s
2400 m³/s
2800 m³/s
3200 m³/s

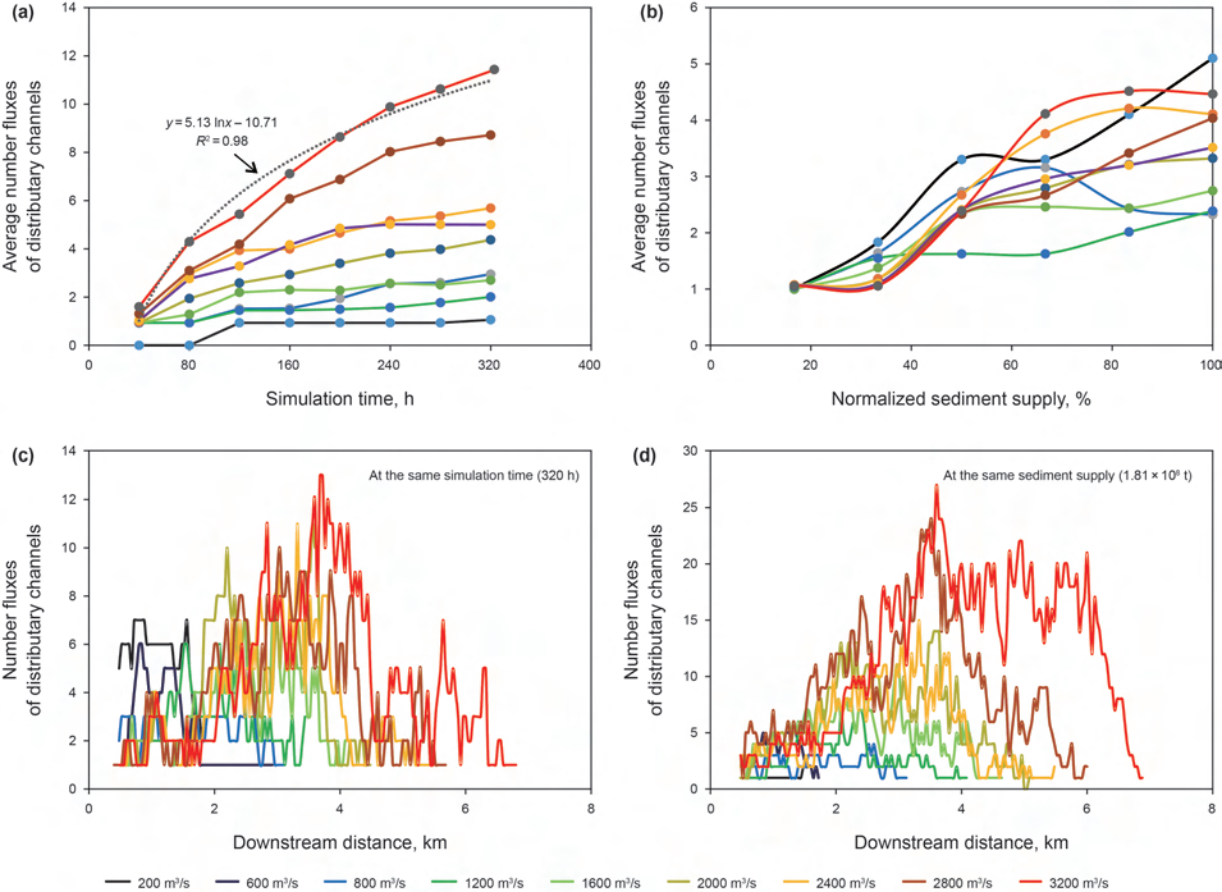
(a)
Average number fluxes of distributary channels
y = 5.13 lnx – 10.71
R² = 0.98
Simulation time, h
(b)
Average number fluxes of distributary channels
Normalized sediment supply, %
(c)
At the same simulation time (320 h)
Number fluxes of distributary channels
Downstream distance, km
(d)
At the same sediment supply (1.81 × 10⁸ t)
Number fluxes of distributary channels
Downstream distance, km
200 m³/s
600 m³/s
800 m³/s
1200 m³/s
1600 m³/s
2000 m³/s
2400 m³/s
2800 m³/s
3200 m³/s